Acta Crystallographica Section D
Biological Crystallography
ISSN 1399-0047

X-ray, spectroscopic and normal-mode dynamics of calexcitin: structure–function studies of a neuronal calcium-signalling protein

P. T. Erskine, A. Fokas, C. Muriithi, H. Rehman, L. A. Yates, A. Bowyer, I. S. Findlow, R. Hagan, J. M. Werner, A. J. Miles, B. A. Wallace, S. A. Wells, S. P. Wood and J. B. Cooper

Acta Cryst. (2015). D**71**, 615–631

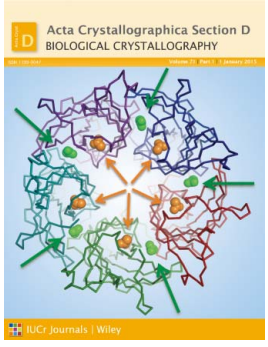

Acta Crystallographica Section D: Biological Crystallography welcomes the submission of papers covering any aspect of structural biology, with a particular emphasis on the structures of biological macromolecules and the methods used to determine them. Reports on new protein structures are particularly encouraged, as are structure–function papers that could include crystallographic binding studies, or structural analysis of mutants or other modified forms of a known protein structure. The key criterion is that such papers should present new insights into biology, chemistry or structure. Papers on crystallographic methods should be oriented towards biological crystallography, and may include new approaches to any aspect of structure determination or analysis. Papers on the crystallization of biological molecules will be accepted providing that these focus on new methods or other features that are of general importance or applicability.

BIOLOGICAL CRYSTALLOGRAPHY

ISSN 1399-0047

X-ray, spectroscopic and normal-mode dynamics of calexcitin: structure–function studies of a neuronal calcium-signalling protein

P. T. Erskine,[a] A. Fokas,[a] C. Muriithi,[a] H. Rehman,[a] L. A. Yates,[b]‡ A. Bowyer,[b] I. S. Findlow,[b] R. Hagan,[b] J. M. Werner,[b] A. J. Miles,[c] B. A. Wallace,[c] S. A. Wells,[d] S. P. Wood[a] and J. B. Cooper[a]*

[a]Laboratory of Protein Crystallography, Centre for Amyloidosis and Acute Phase Proteins, UCL Division of Medicine (Royal Free Campus), Rowland Hill Street, London NW3 2PF, England, [b]Centre of Biological Sciences, University of Southampton, Southampton SO17 1BJ, England, [c]Institute of Structural and Molecular Biology, Birkbeck College, University of London, London WC1E 7HX, England, and [d]Department of Chemistry, University of Bath, Claverton Down, Bath BA2 7AY, England. *Correspondence e-mail: jon.cooper@ucl.ac.uk

Received 16 November 2014
Accepted 4 December 2014

‡ Present address: Division of Structural Biology, Wellcome Trust Centre for Human Genetics, University of Oxford, Oxford OX3 7BN, England.

Keywords: calcium signalling; neuronal plasticity; learning; memory; EF-hand.

PDB references: calexcitin, T188D mutant, 4ndc; T61D+T188D double mutant, 4ndd; T61D mutant, 4ndb

Supporting information: this article has supporting information at journals.iucr.org/d

The protein calexcitin was originally identified in molluscan photoreceptor neurons as a 20 kDa molecule which was up-regulated and phosphorylated following a Pavlovian conditioning protocol. Subsequent studies showed that calexcitin regulates the voltage-dependent potassium channel and the calcium-dependent potassium channel as well as causing the release of calcium ions from the endoplasmic reticulum (ER) by binding to the ryanodine receptor. A crystal structure of calexcitin from the squid *Loligo pealei* showed that the fold is similar to that of another signalling protein, calmodulin, the N- and C-terminal domains of which are known to separate upon calcium binding, allowing interactions with the target protein. Phosphorylation of calexcitin causes it to translocate to the cell membrane, where its effects on membrane excitability are exerted and, accordingly, *L. pealei* calexcitin contains two protein kinase C phosphorylation sites (Thr61 and Thr188). Thr-to-Asp mutations which mimic phosphorylation of the protein were introduced and crystal structures of the corresponding single and double mutants were determined, which suggest that the C-terminal phosphorylation site (Thr188) exerts the greatest effects on the protein structure. Extensive NMR studies were also conducted, which demonstrate that the wild-type protein predominantly adopts a more open conformation in solution than the crystallographic studies have indicated and, accordingly, normal-mode dynamic simulations suggest that it has considerably greater capacity for flexible motion than the X-ray studies had suggested. Like calmodulin, calexcitin consists of four EF-hand motifs, although only the first three EF-hands of calexcitin are involved in binding calcium ions; the C-terminal EF-hand lacks the appropriate amino acids. Hence, calexcitin possesses two functional EF-hands in close proximity in its N-terminal domain and one functional calcium site in its C-terminal domain. There is evidence that the protein has two markedly different affinities for calcium ions, the weaker of which is most likely to be associated with binding of calcium ions to the protein during neuronal excitation. In the current study, site-directed mutagenesis has been used to abolish each of the three calcium-binding sites of calexcitin, and these experiments suggest that it is the single calcium-binding site in the C-terminal domain of the protein which is likely to have a sensory role in the neuron.

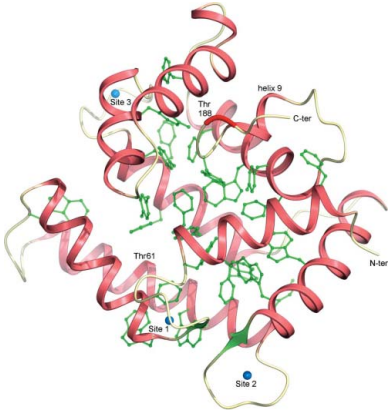

1. Introduction

The protein calexcitin was originally identified in the photoreceptor neurons of the marine snail *Hermissenda crassicornis* as a ~20 kDa cytosolic protein that became up-regulated and phosphorylated following a Pavlovian training protocol (Nelson *et al.*, 1990). *Hermissenda* are normally attracted

towards light but are repelled by movement, which causes foot retraction. The snails become conditioned to retract upon exposure to light (normally an attractive stimulus) if they are simultaneously exposed to both light and movement (*e.g.* on an illuminated turntable). The up-regulation of calexcitin was correlated with exposure to both light and movement and not with each separate stimulus alone. Electrophysiological studies involving micro-injection of the purified calexcitin protein into *Hermissenda* photoreceptors showed that it regulated the voltage-dependent potassium channel and the calcium-dependent potassium channel and was capable of reproducing the electrophysiological effects of learning in neurons. The protein was found to bind calcium and there is evidence that it has GTPase activity (Alkon & Nelson, 1990; Nelson *et al.*, 1994).

Calexcitin was first isolated from the optic lobe of the long-finned squid *Loligo pealei* (Nelson *et al.*, 1996). It has been shown that the protein kinase C (PKC)-dependent phosphorylation of calexcitin causes it to translocate to the cell membrane, where its effects on membrane excitability are exerted (Nelson & Alkon, 1995). Accordingly, *L. pealei* calexcitin contains two PKC phosphorylation consensus sequences and is a good substrate for PKC *in vitro* (Nelson & Alkon, 1995; Gombos *et al.*, 2001). In neuronal cells, the activation of PKC or an increase in intracellular Ca^{2+} can cause long-term inhibition of K^+ currents and it is possible that calexcitin is involved in these processes. Calexcitin causes the release of calcium ions from the endoplasmic reticulum (ER) by binding to and activating ryanodine receptors (Cavallaro *et al.*, 1997), which form one of the main channels for Ca^{2+} release from the ER. Calexcitin has been shown to co-purify with squid ryanodine receptors and the interaction between these two proteins is calcium-dependent (Nelson *et al.*, 1999). Phosphorylation of calexcitin by PKC was found to inhibit the interaction with the ryanodine receptor.

Cloning and sequencing of squid calexcitin cDNA showed that the protein consists of 191 amino acids and has sequence similarity to several sarcoplasmic calcium-binding proteins (SCPs; Nelson *et al.*, 1996). There are three Ca^{2+}-binding sites in calexcitin, and titration studies have indicated that the protein has two apparent affinities for calcium, the higher of which has a K_d of $\sim$40 n*M*. This must be owing to tight calcium-binding sites which will be occupied even when the neuron is at resting potential (Ca^{2+} concentation in the nanomolar to 0.1 µ*M* range; Ascoli *et al.*, 1997). The protein has another measurable calcium affinity, referred to as the regulatory site or sensor site, with a K_d that has been estimated at just below 1 µ*M* and this is in the concentration range for bulk calcium during neuronal activation.

The evidence that calexcitin is a GTPase (Nelson *et al.*, 1996) would make this a remarkable, and possibly unique, protein with dual functions both as a calcium sensor and a G protein. Whilst the early reports of the GTPase activity were contested by another group (Gombos *et al.*, 2001), more recent reports suggest that the GTPase activity of calexcitin is stimulated by calcium in several species, most notably *Drosophila* (Nelson *et al.*, 2003). Calcium ions are known to bind to the protein with submicromolar affinity and they induce significant conformational changes within the physiological Ca^{2+} concentration range. This has been demonstrated by circular dichroism (CD), fluorescence, NMR and infrared spectroscopy (Gombos *et al.*, 2001; Ascoli *et al.*, 1997). Calexcitin shares significant sequence identity (almost 40%) with juvenile hormone diol kinase (JHDK), an insect enzyme that uses ATP or GTP to phosphorylate its polyisoprene substrate (Maxwell, Welsh, Horodyski *et al.*, 2002; Maxwell, Welch & Schooley, 2002; Li *et al.*, 2005). Intriguingly, the activity of JHDK is inhibited by the presence of calcium, suggesting that the calcium-free or partly decalcified form of the protein may be the catalytically active species.

The three-dimensional structure of *L. pealei* calexcitin has been determined by X-ray analysis at a resolution of 1.8 Å (Beaven *et al.*, 2005; Erskine *et al.*, 2006). The overall structure is predominantly helical and compact, with a pronounced hydrophobic core between the N- and C-terminal domains of the molecule. The structure consists of four EF-hand motifs (numbered 1–4 from the N-terminus to the C-terminus), although only the first three EF-hands are involved in binding calcium ions since the C-terminal EF-hand (number 4) lacks the amino acids required for calcium binding. The overall structure is quite similar to that of the sarcoplasmic calcium-binding protein from *Amphioxus* (ASCP), although the sequence identity is low at 31% (Cook *et al.*, 1993; Vijay-Kumar & Cook, 1992). The structure showed that the two amino acids of calexcitin which are known to be phosphorylated by protein kinase C are close to the domain interface and thus phosphorylation is likely to regulate the opening of the domains that is probably required for binding to target proteins. The residues which have been implicated in the GTPase activity of calexcitin by mutagenesis are in a short but highly conserved region of 3_{10}-helix close to the C-terminus. This helix resides in a large loop that is partly sandwiched between the N- and C-terminal domains, suggesting that GTP binding may also require or may cause domain opening. The structure possesses a pronounced electropositive crevice in the vicinity of the 3_{10}-helix that might provide an initial docking site for the triphosphate group of GTP.

In this paper, we report a number of biophysical and structural studies of site-directed mutants of calexcitin which were designed to probe the role of its calcium-binding and phosphorylation sites. An invariant feature of the EF-hand motif is that one of the acidic amino acids which coordinate the calcium ion does so using both of its carboxylate O atoms. Mutation of the corresponding aspartate or glutamate residue to an asparagine or glutamine, respectively, has been shown to significantly reduce the affinity of the affected site for calcium ions, effectively abolishing the site, with the minimum of perturbation to the surrounding protein structure (Starovasnik *et al.*, 1991; Maune, Beckingham *et al.*, 1992; Maune, Klee *et al.*, 2002; Martin *et al.*, 1992). Accordingly, we have engineered the mutations D34N, E85Q and E130Q which affect the bidentate ligands in each of the three calcium-binding sites of calexcitin, the first two of which reside in the N-terminal domain of the protein (sites 1 and 2) and the last in

the C-terminal domain (site 3). The affinity of each of these mutants for Ca^{2+} ions has been measured by calcium-titration experiments using tryptophan fluorescence in order to discern which of the sites is likely to have a calcium-sensory role in the neuron. The sensory site would be expected to have an affinity just below the micromolar range, whereas the higher affinity calcium-binding sites have been shown to have an affinity in the nanomolar range. *In vivo*, calexcitin can be phosphorylated by PKC at two positions (Thr61 and Thr188) and this is linked to changes in its electrophysiological effects (Nelson & Alkon, 1995). Whilst O-linked phosphorylation of proteins can occur at serine, threonine and tyrosine residues in eukaryotic cells, *Escherichia coli* is unable to phosphorylate these amino acids. For proteins which are expressed in *E. coli*, one common way to mimic phosphorylation is to mutate the corresponding residues to one of the negatively charged amino acids aspartate or glutamate, which resemble the charge state of a phosphorylated side chain. Accordingly, we have engineered T61D and T188D mutations in calexcitin and repeated the calcium-titration experiments to assess the effects of phosphorylation on the calcium-binding behaviour of the protein, and have determined the crystal structures of these two mutants as well as the corresponding double mutant. We have also carried out pebble-game rigidity analysis and normal-mode-biased geometric simulations on wild-type and mutant structures in order to explore the constraint network, and the capacity for flexible motion, of calexcitin. Rigidity analysis is advantageous in identifying the network of noncovalent interactions in the protein and their effect in stabilizing and constraining the crystal structure (Jacobs *et al.* 2001). In this case we obtain particularly interesting results on the interactions between the N-terminal and C-terminal domains. Geometric simulations biased along low-frequency normal-mode directions (Jimenez-Roldan *et al.*, 2012) are a rapid and efficient method to explore the intrinsic flexibility of a protein crystal structure by generating variant structures with the same local covalent and noncovalent bonding geometry as the crystal. The results are useful both practically in reconciling static and dynamic structural data and conceptually in visualizing the protein as an intrinsically flexible and dynamic macromolecule rather than a 'frozen' crystal structure.

2. Materials and methods

2.1. Mutagenesis, expression and crystallization of mutant calexcitins

Expression, nickel-affinity purification, crystallization and structure determination of wild-type *L. pealei* calexcitin has been described previously (Beaven *et al.*, 2005; Erskine *et al.*, 2006). The QuikChange mutagenesis system (Agilent Technologies) was used to introduce the desired base changes into the pET-16b calexcitin expression construct (a kind gift from Professor Dan Alkon, Blanchette Rockefeller). The following mutagenic primers were obtained from Integrated DNA Technologies (Coralville, USA) for the EF-hand mutations (D34N, E85Q and E130Q), where the 'f' and 'r' suffixes indicate the forward and reverse primers, respectively: D34Nf, GGCGGGTCATTGAATGGGATAATTTTGAGCTGGCC; D34Nr, GGCCAGCTCAAAATTATCCCATTCAATGACGCC; E85Qf, GAGCAAGTTACTAAAGAGCAATGGCTGAAGATGTGGGCC; E85Qr, GGCCCACATCTTCAGCCTATGCTCTTTAGTAACTTGCTC; E130Qf, GGTGACAACATTATTGACAAACATCAGTACAGTACTGTC; E130Qr, GACAGTACTGTACTGATGTTTGTCAATAATGTTGTCACC. The following primers were ordered from Eurogentec (Liege, Belgium) for the phosphorylation-mimic mutations (T61D and T188D): T61Df, GAGGCCAGAGCTGACCTGAAACTCATCTGGG; T61Dr, CCCAGATGAGTTTCAGGTCAGCTCTGGCCTC; T188Df, GGGGCTAAGGGC AACCATCTGTTTGGTGACCTAAAACTTTAA; T188Dr, TTAAAGTTTTAGGTCACCAAACAGATGGTTGCCCTTAGCCCC. Each mutagenesis reaction was undertaken using a Techne Progene thermal cycler and each point mutation was confirmed by DNA sequencing (DNA Sequencing and Services, Dundee, Scotland). All possible double mutants of the metal-binding sites (D34N+E85Q, D34N+E130Q and E85Q+E130Q) and the phosphorylation sites (T61D+T188D) were engineered by repeating the above process on DNA which had already been mutagenized once and were confirmed again by sequencing. The mutant DNA was transformed into *E. coli* BL21(DE3) cells for expression in LB medium. Cells were grown at 37°C to mid-log phase in LB medium with 50 µg ml^{-1} ampicillin and were then induced by the addition of isopropyl β-D-1-thiogalactopyranoside (IPTG) to a final concentration of 1 m*M* and grown overnight at 37°C. In one case where the mutant protein was found in inclusion bodies (E130Q), the expression was repeated as above except that the cells were given a 30 min heat shock at 42°C followed by cooling for 5 min on ice prior to induction with IPTG and growth at 16°C for 2 d. The resulting cell cultures were pelleted and lysed by sonication in a buffer consisting of 50 m*M* Tris pH 7.5, 100 m*M* NaCl, 1 m*M* $CaCl_2$ prior to ultracentrifugation at 40 000*g* for 40 min. The subsequent purification of the His-tagged protein from the supernatant involved the use of HisTrap 1 ml nickel-affinity columns (GE Healthcare), from which the protein was eluted with 250 m*M* imidazole. The affinity-purified protein was then re-equilibrated with the lysis buffer and concentrated to 3 mg ml^{-1} using a Vivaspin centrifugal concentrator (GE Healthcare) with a 10 kDa cutoff. Crystals of the T61D, T188D and T61D+T188D mutant calexcitins were grown by the vapour-diffusion method using the conditions reported for the wild-type protein (Beaven *et al.*, 2005). This involved mixing 5 µl protein solution at a concentration of 3 mg ml^{-1} with 5 µl well solution consisting of 15–40%(*w*/*v*) PEG 4000, 100 m*M* sodium citrate pH 5.5–7.0, 200 m*M* ammonium acetate. Large crystals of up to 1 mm in their longest dimension appeared within 2–3 weeks at room temperature. The crystals were mounted in loops with approximately 30%(*v*/*v*) glycerol added as a cryoprotectant and flash-cooled in a nitrogen-gas cryostream at 100 K. Data collection using a PILATUS detector at station I04-1 of the Diamond synchrotron revealed that the crystals were orthorhombic and belonged to space

group $P2_12_12_1$. Data processing with *MOSFLM* (Leslie, 2006), *SCALA* (Evans, 2006) and other programs in the *CCP*4 suite (Winn *et al.*, 2011) yielded intensity data to high resolution (for details, see Table 1). The crystals contained two calexcitin monomers per crystallographic asymmetric unit. Since the T61D mutant had the same unit-cell parameters as the wild-type protein, the structure was refined directly using *REFMAC* (Murshudov *et al.*, 2011). However, the T188D mutant had an appreciably different unit cell and structure analysis therefore proceeded by molecular replacement using *MOLREP* (Vagin & Teplyakov, 2010) with a monomer of the wild-type protein as the search model. Refinement was undertaken as for the other mutants, with introduction of the mutant residue(s) and other manual rebuilding performed using *Coot* (Emsley & Cowtan, 2004). The $R_{\rm free}$ reflection set was chosen using *SHELXPRO* (Sheldrick & Schneider, 1997) in thin resolution shells to avoid bias between the working and test sets owing to the presence of noncrystallographic symmetry. Except for the initial round of refinement, in which rigid-body constraints were applied to both monomers in the asymmetric unit, noncrystallographic symmetry (NCS) restraints were not used. The refinement statistics of the final model are shown in Table 1. Validation tests were performed using *PROCHECK* (Laskowski *et al.*, 1993), *SFCHECK* (Vaguine *et al.*, 1999) and *MolProbity* (Lovell *et al.*, 2003; Chen *et al.*, 2010). Figures showing molecular structures were prepared using *CueMol* (http://www.cuemol.org/en) and *POV-Ray* (http://www.povray.org). The coordinates and structure factors for the T61D, T188D and double mutant constructs have been deposited in the Protein Data Bank and assigned accession numbers 4ndb, 4ndc and 4ndd, respectively.

Table 1
X-ray crystallographic and data-processing statistics for the mutants of calexcitin.

Values in parentheses are for the outer resolution shell.

Mutant	T61D	T188D	T61D+T188D
Space group	$P2_12_12_1$	$P2_12_12_1$	$P2_12_12_1$
Unit-cell parameters			
a (Å)	47.2	46.0	46.8
b (Å)	69.2	68.0	69.4
c (Å)	135.4	125.9	133.5
Resolution (Å)	27.9–2.0 (2.1–2.0)	28.2–2.0 (2.1–2.0)	46.8–2.9 (3.1–2.9)
$R_{\rm merge}$† (%)	7.7 (34.7)	10.4 (53.8)	9.4 (53.0)
$R_{\rm meas}$‡ (%)	8.4 (37.8)	11.4 (59.1)	10.7 (59.9)
$CC_{1/2}$§ (%)	99.7 (93.4)	99.7 (76.9)	99.5 (78.5)
Completeness (%)	98.2 (98.2)	95.4 (94.4)	98.4 (99.5)
Average $I/\sigma(I)$	16.0 (5.2)	10.6 (3.1)	13.9 (3.9)
Multiplicity	6.5 (6.4)	6.1 (5.8)	4.6 (4.6)
Mosaicity (°)	0.3	1.0	0.8
R factor (%)	16.3	17.0	17.1
$R_{\rm free}$ (%)	21.2	22.4	28.3
Total unique reflections	28737	24739	9359
R.m.s.d., bond lengths (Å)	0.02	0.02	0.01
R.m.s.d. bond angles (°)	1.9	1.8	1.6

† $R_{\rm merge} = \sum_{hkl}\sum_i |I_i(hkl) - \langle I(hkl)\rangle| / \sum_{hkl}\sum_i I_i(hkl)$. ‡ $R_{\rm meas} = \sum_{hkl}\{N(hkl)/[N(hkl)-1]\}^{1/2}\sum_i |I_i(hkl) - \langle I(hkl)\rangle| / \sum_{hkl}\sum_i I_i(hkl)$, where $\langle I(hkl)\rangle$ is the mean intensity of the $N(hkl)$ observations $I_i(hkl)$ of each unique reflection hkl after scaling. § $CC_{1/2}$ is the half-set correlation coefficient as described by Karplus & Diederichs (2012).

2.2. Calcium-titration experiments

Aliquots of the concentrated protein were dialysed against a 2 l volume of 1 m*M* EGTA for 24 h to remove calcium ions bound to the protein. After 24 h, the EGTA solution was exchanged for 2 l deionized water and left for a further 24 h. The decalcified protein was then re-concentrated, as above, to 2 mg ml^{-1}. The calcium-binding affinities of the mutants were then determined using a fluorescence-based calcium-titration assay. A range of stock calcium solutions of precise molarity were made by dissolving calcium carbonate in water by the dropwise addition of 10 *M* HCl. Similarly, a stock solution of 0.15 *M* EGTA was made by the dropwise addition of 10 *M* NaOH to dissolve the chelating agent. For the fluorescence measurements, 10 µl decalcified protein at 2 mg ml^{-1} and 10 µl 0.15 *M* EGTA were added to 980 µl 50 m*M* HEPES pH 7.5, 0.1 *M* KCl in a quartz cuvette followed by mixing. The fluorescence spectrum was then recorded using an excitation wavelength of 295 nm with a Shimadzu RF-500 IPC spectrofluorometer and the fluorescence emission intensity in the wavelength range 305–400 nm was integrated. Following this, 2 µl volumes of each of the calcium stock solutions were added to the cuvette prior to mixing and equilibration at 25°C. At each calcium ion concentration, the fluorescence spectrum was recorded as above. The total free concentration of calcium ions for each measurement was calculated using *MAXCHELATOR* (Bers *et al.*, 1994).

2.3. Circular-dichroism (CD) spectroscopic studies

The phosphorylation-mimic mutants and wild-type calexcitin were transferred to 50 m*M* phosphate buffer pH 7.5 with 1 m*M* $CaCl_2$ and 10 µ*M* β-mercaptoethanol present. CD spectra were recorded using an Aviv 62DS instrument over a wavelength range from 280 to 180 nm using a 1 nm interval and a dwell time of 1 s at a temperature of 25°C. Cylindrical quartz Suprasil optical cells (Helma UK Ltd) with path lengths of 0.0015, 0.0024 and 0.005 cm were used. In each case, three replicate sample spectra were measured. Three replicate baseline spectra (consisting of the buffer without protein) were also obtained. The replicate sample spectra were averaged and the averaged baseline spectrum was subtracted from each of them. The subtracted spectra were calibrated against the spectrum of camphorsulfonic acid (Miles *et al.*, 2003) and scaled to units of $\Delta\varepsilon$ using mean residue weights of 117.2 for the wild type, 117.3 for the single mutants and 117.4 for the double mutant. Processing was carried out using the *CDtool* software (Lees *et al.*, 2004) and secondary-structure analyses were performed using the *DichroWeb* analysis server (Whitmore & Wallace, 2008). The proportion of helix was determined as the average of values from the *CONTINLL* (Van Stokkum *et al.*, 1990), *SELCON*3 (Sreerama *et al.*, 1999) and *CDDSTR* (Sreerama & Woody, 2000) algorithms, which were used with the SP175t reference data set (Lees *et al.*, 2006). The CD spectra and metadata have been deposited in the Protein Circular Dichroism Data Bank (PCDDB) located at http://

pcddb.cryst.bbk.ac.uk/home.php as entries CD0004676000 to CD0004679000.

2.4. NMR studies

Uniformly labelled recombinant calexcitin was over-expressed in *E. coli* BL21(DE3) cells grown solely on M9 medium supplemented with 1 g l^{-1} $^{15}NH_4Cl$ and 2 g l^{-1} $^{13}C_6$-D-glucose. Prior to induction, the cultures were incubated at 37°C before being cooled to 30°C and subsequently incubated with 1 m*M* IPTG for 18 h. The cells were harvested and the labelled calexcitin was purified as described previously. NMR samples were prepared as 1 m*M* calexcitin in 20 m*M* bis-tris, 50 m*M* KCl, 10 m*M* $CaCl_2$, 1 m*M* dithiothreitol (DTT) pH 7 containing 0.05% NaN_3 in 600 µl 5% D_2O in H_2O for assignment purposes. Such samples were diluted with the aforementioned buffer to half of the original calexcitin concentration for relaxation and residual dipolar coupling (RDC) measurements. Aligned samples were prepared by adding a pre-dried 600 µl volume, 5 mm diameter, 5% polyacrylamide gel to a 600 µl 0.5 m*M* calexcitin sample and allowing the gel to swell for 48 h at 4°C prior to insertion into a 5 mm NMR tube and data collection.

All NMR experiments were performed on a Varian Inova 600 MHz spectrometer at 25°C equipped with a room-temperature 5 mm triple-resonance probe. Backbone assignments of Ca^{2+}–calexcitin were achieved using three-dimensional HNCACB (Kay *et al.*, 1994; Wittekind & Mueller, 1993) and CBCACONH (Grzesiek & Bax, 1992) experiments. The RDC data were used to investigate the solution structures of the calexcitin domains and their relative orientations. NMR data recorded on aligned samples revealed negligible chemical shift changes when compared with the isotropic data, indicating the effects of the gel matrix on the protein structure to be minimal. $[^1H]$–^{15}N dipolar couplings were recorded from 0.5 m*M* calexcitin samples using two-dimensional IPAP-type sensitivity-enhanced experiments (Ottiger *et al.*, 1998) with an acquisition time of 152 ms in the nitrogen dimension. The errors in the RDCs were estimated to be 0.5 Hz. Alignment tensors were calculated for each calexcitin domain (N-domain including residues 2–100 and C-domain including residues 101–191) from $[^1H]$–^{15}N RDC data in secondary-structural elements using the program *Module*. This allowed 32 and 36 RDCs to be resolved in the N-terminal and C-terminal calexcitin domains, respectively, for the major conformer excluding glycine and loop residues. The resulting alignment tensors of the N-terminal and C-terminal domains were rotated into a common coordinate frame by rigid-body rotation of the C-terminal domain about Ser102. A minor conformational state for calexcitin was treated the same way; however, combining RDC measurements from the alternative conformational state residues (that could be observed) with those of the major conformer was deemed to be too unreliable an approach since weak peaks from the minor conformer may simply be masked by the major conformer and therefore the resulting RDC set would be incorrect.

^{15}N relaxation time constants were calculated from a series of seven two-dimensional ^{15}N T_1 and T_2 relaxation spectra (Kay *et al.*, 1992; Farrow *et al.*, 1994) recorded with relaxation delays of 0.02, 0.08, 0.16, 0.32, 0.6, 1.0 and 1.4 s and 0.01, 0.03, 0.05, 0.07, 0.09, 0.11 and 0.13 s for T_1 and T_2, respectively. The data were processed with mild resolution enhancement and zero-filling in the proton dimension and linear prediction in nitrogen. All data were processed using *NMRPipe* and *NMRDraw* (Delaglio *et al.*, 1995) and were analyzed using *NMRview* (Johnson & Blevins, 1994). Rotational correlation times were calculated from the average T_1:T_2 ratio of residues in secondary-structural elements only. Rotational correlation time predictions using hydrodynamic modelling were made directly from PDB structures or models with *HYDRONMR* (García de la Torre *et al.*, 2000) using a temperature of 25°C and a bead size of 3.2 Å.

Samples of calexcitin in the presence of GTP, GDPNP and a synthetic pepide (Ac-LLPNTQSFPNC-NH_2) mimicking part of the ryanodine receptor which is reported to interact with calexcitin (Nelson *et al.*, 1999) were prepared at a ligand: protein ratio of 20:1 with a calexcitin concentration of 0.1 m*M* in the buffer defined above. Chemical shift differences were mapped from ^{15}N HSQC spectra collected as described above.

2.5. Rigidity analysis and flexible motion simulations

Rigidity in calexcitin was explored using pebble-game rigidity analysis as implemented in the software *FIRST* (Jacobs *et al.*, 2001), identifying polar and hydrophobic tether interactions and dividing the structure into rigid clusters based on the distribution of constraints and degrees of freedom. The inclusion of polar interactions is controlled by an energy-cutoff parameter ranging from 0 to −4 kcal mol^{-1} to obtain comparative information on the rigidity of different regions of the protein. Manual removal of interdomain constraints, when required, was achieved by editing the constraint lists used by *FIRST*.

Flexible motion was explored using template-based geometric simulation as implemented in the *FRODA* module of *FIRST* (Wells *et al.*, 2005). Motion was explored along low-frequency normal-mode directions calculated using a coarse-grained (one site per residue) representation of the protein structure with the elastic network modelling software *ElNémo* (Suhre & Sanejouand, 2004). In the construction of the elastic network, springs of uniform strength were placed between all α-carbon positions lying within a 12 Å distance cutoff and eigenvectors were obtained for the ten lowest frequency nontrivial normal modes (modes 7–16, as modes 1–6 are trivial rigid-body motions). Residues 1–5 in the N-terminus were deleted from the structure, as otherwise multiple modes localize on this relatively unstructured section of the molecule. In the normal-mode biased geometric simulations (Jimenez-Roldan *et al.*, 2012), motion was explored parallel and anti-parallel to each eigenvector using a directed step size of 0.01 Å for a total of 1000 steps in each trajectory, saving every 100th step as a frame for analysis; this was sufficient to project all modes until their amplitude was limited by constraints in the structure. The constraint network for flexible motion included polar interactions stronger than −3 kcal mol^{-1}.

Simulations of a cleft-opening motion along the mode 7 direction were carried out with a constraint network edited to remove interdomain noncovalent constraints. For this simulation a smaller bias and a longer simulation trajectory were used: a directed step size of 0.001 Å and a total of 100 000 steps, saving every 500th step as a frame for analysis.

3. Results

All possible single and double mutants of the bidentate ligand residue at the three calcium-binding sites of *L. pealei* calexcitin were engineered and expressed in *E. coli*. The single-site mutants were expressed at high levels and were purified for calcium-binding studies. However, out of the three double-site mutants (sites 1 and 2, 1 and 3, and 2 and 3), only the mutant with sites 1 and 2 altered (D34N+E85Q) could be expressed in soluble form and this, too, could not be purified adequately for calcium-binding studies. The other metal-site double mutants, *i.e.* that affecting sites 1 and 3 and that affecting sites 2 and 3, both formed inclusion bodies and refolding was not attempted. In contrast, the phosphorylation-mimic mutants (T61D, T188D and T61D+T188D) could all be expressed in high yield and crystallized for X-ray structure analysis.

3.1. Quality control of the structures

The crystal structures of the phosphorylation-mimic mutations possess two molecules of calexcitin in the asymmetric unit, with solvent contents of 44.8, 38.1 and 43.7% for the T61D, T188D and T61D+T188D mutants, respectively. The corresponding structural models for these three mutants, which have been refined using data to resolutions of 2.0, 2.0 and 2.9 Å, have R factors of 16.3, 17.0 and 17.1%, with $R_{\rm free}$ values of 21.2, 22.4 and 28.3%, respectively (see Table 1). The mutant structures superimpose closely with the best-defined moiety of the wild-type protein (Erskine *et al.*, 2006), with low r.m.s. deviations of 0.2, 0.4 and 0.4 Å, respectively, for the whole protein, and have reasonable mean isotropic temperature factors for all protein atoms of 17.6, 20.2 and 27.4 Å^2, respectively. The final structures have 98.7, 98.4 and 88.7% of

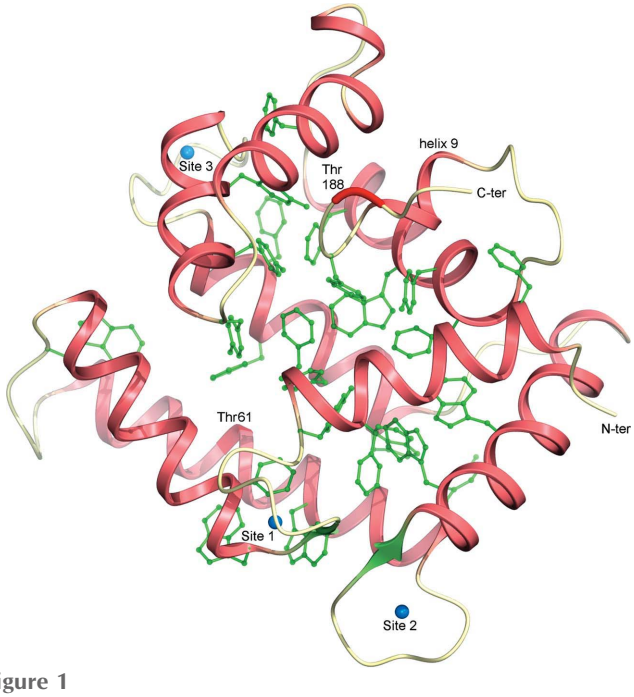

Figure 1
The calcium-binding and phosphorylation sites of calexcitin. The tertiary structure of calexcitin is shown with the helices as pink ribbons and the strands coloured green. The three bound calcium ions are shown in pale blue and the positions of the phosphorylated residues (Thr61 and Thr188) within the protein fold are indicated in dark red. The hydrophobic core of the protein is formed by a large number of aromatic residues which are shown in a pale green ball-and-stick representation. The N-terminal domain of the protein (at the bottom of the picture) essentially forms a cup in which the upper C-terminal domain nestles. The 3_{10}-helix close to the C-terminal end (helix 9) is shown towards the top right.

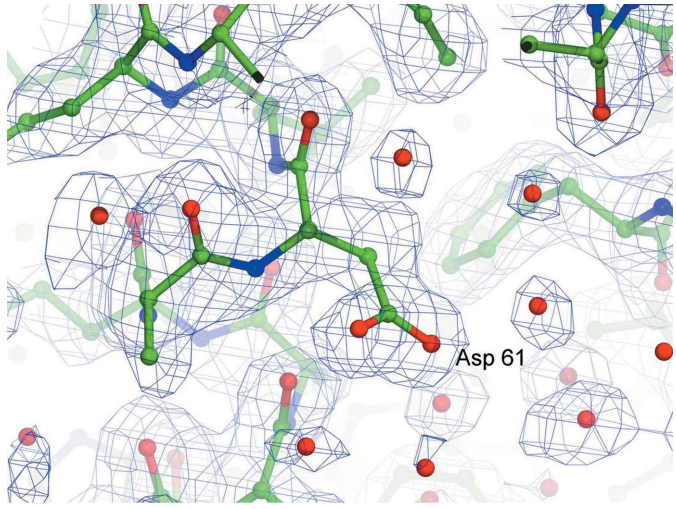

(*a*)

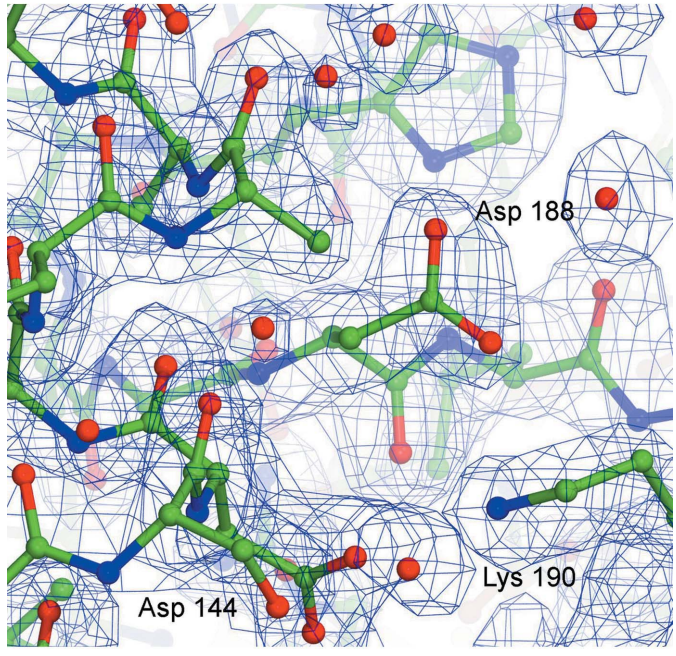

(*b*)

Figure 2
Electron-density maps (2.0 Å resolution) for the phosphorylation-mimic mutations. (*a*) Asp61 of the T61D mutant structure and (*b*) Asp188 of the T188D mutant. Whilst Asp61 is relatively devoid of interactions with the surrounding protein, Asp188 is close to a salt bridge formed by Lys190 and Asp144. The σ_A-weighted electron density shown in blue is contoured at 1.0 r.m.s..

their residues within the 'favoured' regions of the Ramachandran plot by the *MolProbity* criteria and all three have at least 99% of their residues within the 'allowed' boundary. The outlying residues are in regions with poor electron density (at the extreme N-termini and C-termini) and hence their conformations are poorly defined. The isotropic temperature factors for the protein moieties are reasonable except for a few residues at the N-terminal and C-terminal ends of the monomers, where the electron density for a small number of residues remains poor despite extensive efforts to rebuild them throughout the refinement process.

3.2. Structural effects of the phosphorylation-mimic mutations

Calexcitin adopts a compact conformation which is dominated by α-helical secondary-structure elements which assemble to form a pronounced hydrophobic core involving a striking number of closely packed aromatic residues. There are four helix–loop–helix motifs that are formed by helices 1 and 2, 3 and 4, 5 and 6 and finally 7 and 8 which associate together in pairs by antiparallel packing of their constituent α-helices (Fig. 1). The first two helix–loop–helix motifs form the N-terminal domain of the molecule (residues 2–101) and the last two form the C-terminal domain (residues 102–191). The first three helix–loop–helix motifs of calexcitin (formed by helices 1–6) adopt EF-hand folds and are involved in binding calcium ions. In the C-terminal domain there is only one functional metal-binding motif (formed by residues 119–130) since the fourth helix–loop–helix motif lacks the key metal-binding residues. The helices of the two helix–loop–helix motifs in each domain are related by a topological twofold axis which passes in between the Ca^{2+}-binding loops. There are parallels to the structure of calmodulin, a protein with four functional EF-hands. The first two and last two EF-hands of calmodulin form distinct domains that can open upon calcium binding, thereby creating a cleft which allows the molecule to interact with target proteins (see, for example, Rhoads & Friedberg, 1997).

Calexcitin is a substrate for protein kinase C (PKC) and phosphorylation is associated with the translocation of calexcitin to the cell membrane, where its effects on potassium channels are exerted (Nelson *et al.*, 1996). However, phosphorylation of calexcitin has been reported to inhibit its interaction with the ryanodine receptor (Nelson *et al.*, 1999). Interestingly, the phosphorylation of peptides recognized by calmodulin is known to prevent their binding to the protein itself (Minakami *et al.*, 1997; Nakajima *et al.*, 1999). PKC acts at consensus sequences of the form -(Ser/Thr)-*X*-(Arg/Lys)-, and there is evidence that calexcitin is phosphorylated both at Thr61, which lies in the sequence -Thr-Leu-Lys-, and at Thr188, which lies four residues from the C-terminal end of the protein in the same sequence (-Thr-Leu-Lys-; Gombos *et al.*, 2001). Accordingly, the X-ray structure shows that the side chains

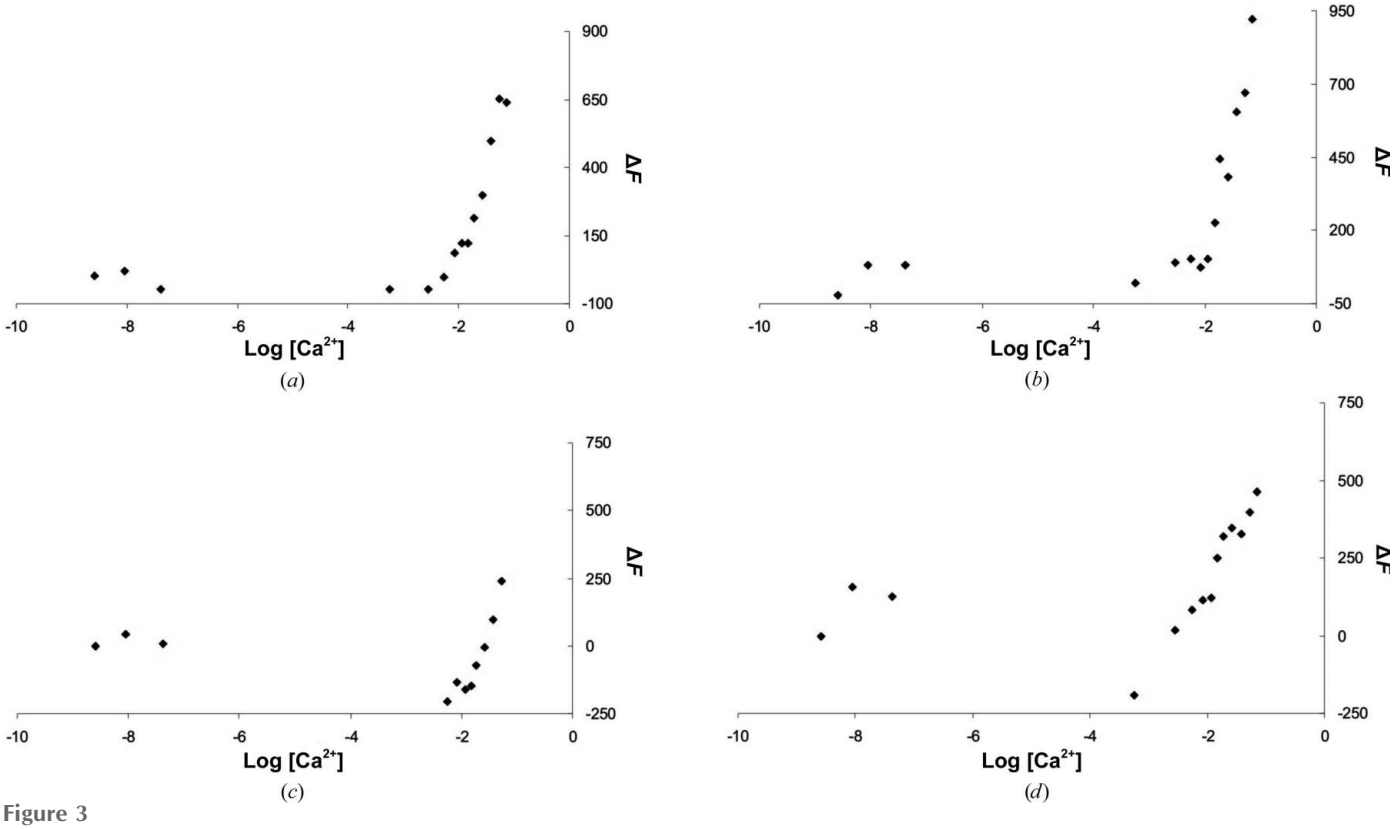

Figure 3
Fluorescence titration curves of the phosphorylation-mimic mutants. (*a*) The change in tryptophan fluorescence as the demetallated protein is titrated with calcium ions is shown for wild-type calexcitin; the titration curves of the T61D, T188D and T61D+T188D mutants are shown in (*b*), (*c*) and (*d*), respectively.

of Thr61 and Thr188 are exposed on the surface of the molecule.

The CD spectra of the wild type and the phosphorylation-mimic mutants were all very similar, and calculations suggested they possess very similar secondary-structure contents (see Supplementary Fig. S1). Indeed, all three mutants crystallized under very similar conditions to native calexcitin. The resulting electron-density maps for the Thr-to-Asp mutants generally define the aspartate residues that are introduced without any ambiguity in the main-chain or side-chain conformation (Fig. 2). Superposition of both monomers of the T61D mutant that are present in the asymmetric unit with the corresponding monomers of the isomorphous wild-type calexcitin structure revealed essentially no change in the structure of the protein. The side chain of the aspartate introduced by this mutation is clearly oriented in the same direction as the side-chain hydroxyl group of the wild-type threonine residue and does not appear to make any additional interactions with the enzyme apart from hydrogen bonds to surrounding water molecules owing to its solvent-exposed disposition. In contrast, the mutation of Thr188 to aspartate seems to introduce an additional salt-bridge interaction with the basic side chain two places along the chain, namely Lys190, arising from a conformational change in this residue. In its new conformation Lys190 can still retain the ionic interaction that it makes with Asp144 in the wild-type structure. A hydrogen bond formed by the side chain of the wild-type Thr188 residue with the main chain of Asp144 is lost in the T188D mutant since the newly introduced aspartate side chain points in the opposite direction. The T188D mutation also introduces other local changes in the structure such as a conformational change in the side chain of the hydrophobic residue two places earlier in the chain, namely Phe186. Indeed, in the second monomer in the asymmetric unit of this mutant structure the Asp188 residue is almost completely disordered, an effect which appears to cause the Phe186 side chain to move considerably and to induce disorder in the neighbouring buried side chain of Trp169.

Whilst the lower resolution of the double-mutant structure warrants some caution in interpretation of the findings, it is clear that the effects observed in the two high-resolution single-mutant structures are substantially replicated in the corresponding double mutant. The most notable effects are concentrated in the vicinity of the T188D mutation which, as mentioned above, induces conformational changes in Trp169 and Asp186, as well as having an additional effect on Tyr110. Very little change from the wild-type structure is seen in the vicinity of the T61D mutation, which suggests that this is unlikely to be the physiologically relevant phosphorylation site. In contrast 'phosphorylation' of Thr188 is found to induce local disruption of the adjacent hydrophobic residues in a region of the molecule which is associated with its putative GTPase activity and is at one of the major electropositive openings into the hydrophobic interdomain cleft of the protein. As a target residue for phosphorylation, it is interesting that Thr188 resides very close to a region of 3_{10}-helix which is formed by residues 181–185 since this is a type of secondary

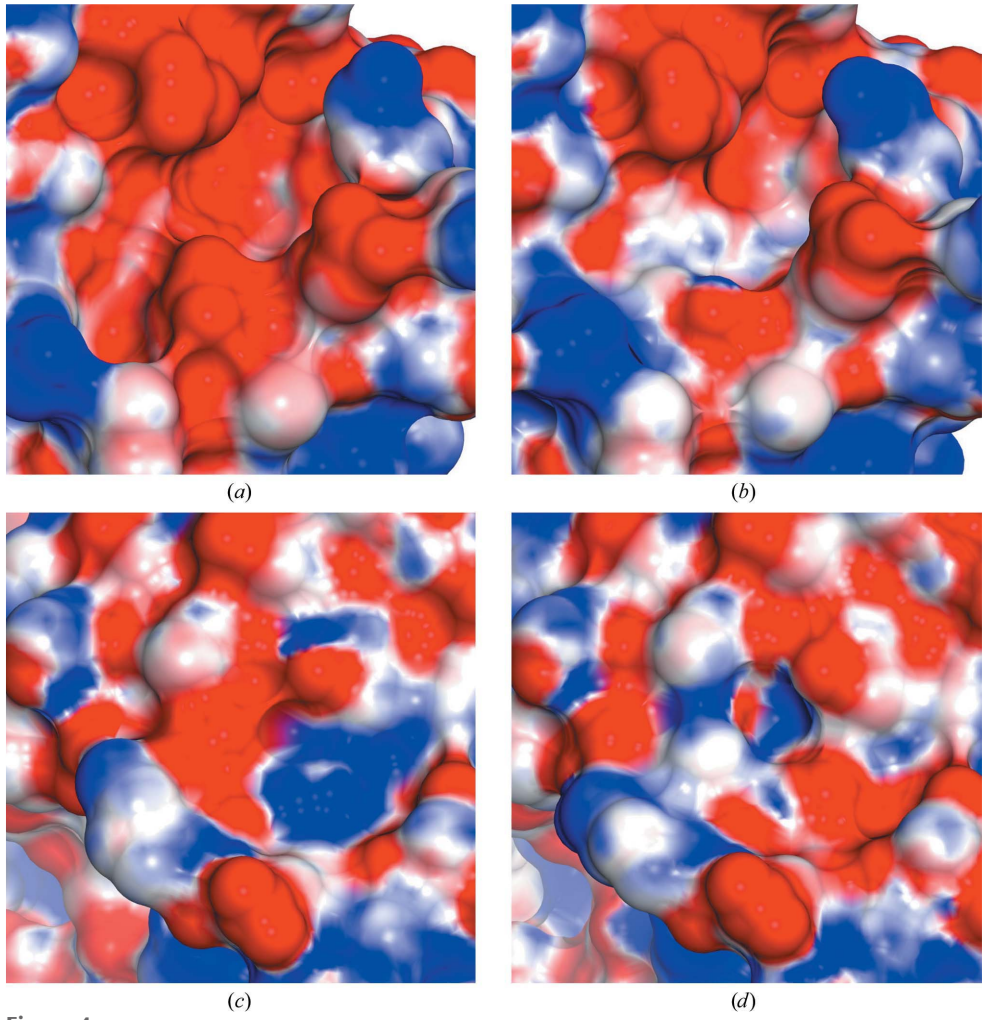

Figure 4
The electrostatic effects of phosphorylation. The solvent-accessible surface of calexcitin showing the electrostatic charge in the vicinity of (*a*) the T61D mutation and (*b*) the wild-type protein for comparison and (*c*) the T188D mutation and (*d*) the same region of the wild-type protein. At physiological pH a phosphate group will have an average charge between −1 and −2, which is greater than that of an aspartate side chain.

structure that is associated with low stability. A similar situation exists for the cyclin-dependent kinase inhibitors p21, p27 and p57, in which phosphorylation of a tyrosine residue within a 3_{10}-helix disrupts the local fold and reduces the ability of the protein to inhibit the associated kinase (Hashimoto *et al.*, 1998).

Fluorescence titration studies suggest that there are no appreciable differences in the calcium-binding properties of the T61D, T188D and T61D+T188D mutant proteins from that of wild-type calexcitin (Fig. 3). This suggests that the physiologically observed phosphorylation of calexcitin is likely to affect the interactions with other proteins in the signalling cascade rather than its metal-binding affinity and is fully in accord with the disposition of the respective sites within the protein. The view shown in Fig. 1 demonstrates that the calcium-binding sites are located at the poles of the protein and the phosphorylation sites are within the equatorial hollowed-out regions that are associated with domain separation and binding to other proteins.

The surface of wild-type calexcitin has pronounced crevices between the N- and C-terminal domains which lead into the hydrophobic core of the molecule. Whilst the electrostatic potential at the protein surface is dominated by acidic residues forming the calcium-binding sites, there is a region of significant positive potential in the immediate vicinity of the C-terminal 3_{10}-helix (helix 9). This arises from a number of conserved basic residues, in particular Lys13 and Arg16, which reside in helix 1 of calexcitin and interact with residues in the 3_{10}-helix. These residues form a positively charged groove between the N-terminal and C-terminal domains that might provide an initial docking site for the triphosphate group of a GTP molecule.

A similar analysis of the phosphorylation-mimetic mutations showed that these residue substitutions appear to markedly alter the local electrostatic potential of the protein in the vicinity of the cleft between the N-terminal and C-terminal domains (Fig. 4). These mutations therefore confer the interdomain groove with a more negatively charged character, which could have implications for ligand binding, although it should be stated that the electrostatics of the protein are still very much dominated by the EF-hand motifs even in the double T61D+T188D mutant. One of the interesting effects of the T188D mutation is that it appears to mask the basicity of His184, which lies within the C-terminal 3_{10}-helix. A strong electrostatic interaction between a phosphate group covalently added to Thr188 and the histidine residue could disrupt the secondary structure of this short helix. Accordingly, the structures demonstrate that the phosphorylation-mimetic mutation of Thr188 has a more disruptive effect on the local protein structure than does the T61D mutation.

3.3. Effects of the calcium-binding site mutations

Calcium-binding studies indicated that calexcitin binds 2–3 Ca^{2+} ions with two apparent dissociation constants: one in the 10^{-7} *M* range and the other in the submillimolar range

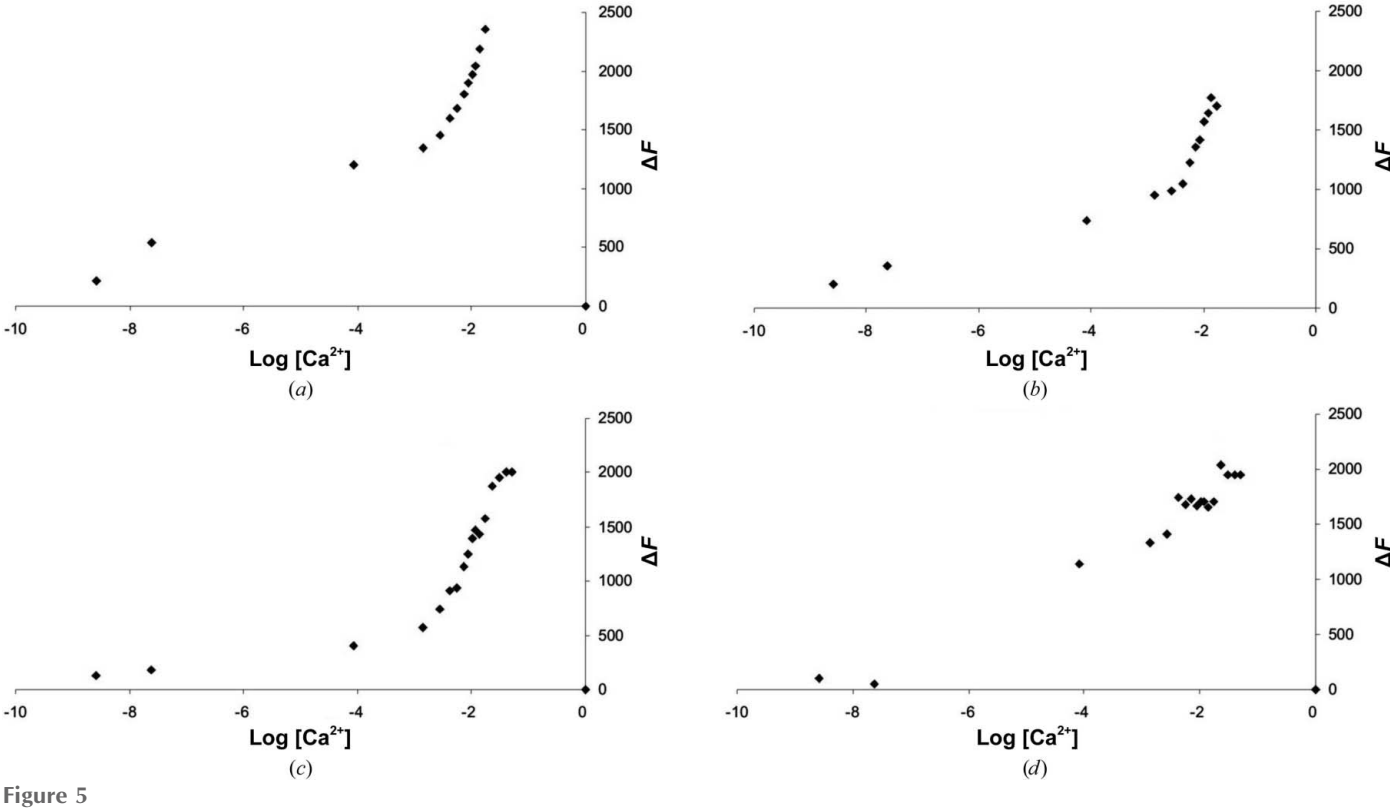

Figure 5
Fluorescence curves of the EF-hand mutants. The change in tryptophan fluorescence as the demetallated protein is titrated with calcium ions is shown for wild-type calexcitin in (*a*) with the titration curves of the D34N (site 1), E85Q (site 2) and E130Q (site 3) mutants shown in (*b*), (*c*) and (*d*), respectively.

(Gombos *et al.*, 2001; Ascoli *et al.*, 1997). Whilst the highest affinity Ca^{2+} sites are quite likely to be fully occupied even at the resting potential of the neuron, sites of near-millimolar affinity are likely to be regulatory sites or sensory sites that would only be occupied during neuronal activation. Calcium binding at a sensor site probably triggers a conformational change, ultimately allowing calexcitin to bind to a target molecule in a signalling pathway. Indeed, CD spectroscopy has shown that calcium binding causes conformational changes leading to an increase in the α-helical content of the protein (Ascoli *et al.*, 1997). There are parallels to the structure of calmodulin (a four EF-hand protein) in which the first two and last two EF-hands form distinct domains that separate when calcium is bound, allowing interactions with target proteins. Most commonly, a segment of the target protein binds in the hydrophobic cleft between the N-terminal and C-terminal domains of calmodulin as an α-helix (Rhoads & Friedberg, 1997). It is worth noting that whilst calexcitin appears to form a fairly closed structure in the crystal, many studies of calmodulin have shown that it is more open and has a greater degree of domain flexibility.

Since the X-ray structure of wild-type calexcitin reveals three well ordered calcium sites that appear to be fully occupied by Ca^{2+} ions, this raises the question as to which of these sites fulfill the sensory or regulatory role, as opposed to simply providing a high-affinity site that is occupied by calcium regardless of the activation state of the neuron. Consequently, we engineered and expressed a series of site-directed mutants of calexcitin (D34N, E85Q and E130Q) which abolish binding at each of the calcium sites (sites 1, 2 and 3, respectively).

The binding of calcium to wild-type and mutant calexcitin was monitored using intrinsic tryptophan fluorescence to follow calcium binding to fully demetallated protein. The resulting fluorescence titration curves shown in Fig. 5 suggest that mutation of either of the EF-hands in the N-terminal domain (site 1 or 2) does not appreciably affect the calcium-binding properties of the protein at either high or low calcium concentrations. In contrast, mutation of the third EF-hand, which resides in the C-terminal domain of the protein, appears to abolish the lowest affinity binding of calcium. This would suggest that the third EF-hand (site 3) is the physiological calcium-sensor site which allows the protein to respond to changes in calcium-ion concentration during neuronal activation. The close association of the two EF-hands in the N-terminal domain presumably allows them to associate very tightly with calcium and therefore they are likely to be occupied even when the neuron is in the resting state. In the mutagenesis experiments, when either site 1 or 2 is mutated the highly cooperative nature of the folding of this domain may compensate for the lack of either one of the two calcium-binding sites; hence, the tryptophan-fluorescence changes that are observed during the addition of calcium to demetallated protein are substantially the same as the wild-type protein. In contrast it is very likely that site 3 is the low-affinity sensor site owing to its lack of a partner calcium-binding loop within the C-terminal domain.

3.4. NMR studies of calexcitin

Backbone assignment of calexcitin in solution immediately revealed the presence of at least two species by the presence of a distinct subset of resonances distributed throughout the protein but most prominent around the first calcium-binding site between residues Thr20 and Lys40 (Fig. 6). The second most populated conformer exists only as 10–20% of the total protein present and does not seem to vary with calexcitin concentration. From NMR signals exhibiting slow exchange in HSQC spectra, we estimate exchange between these states to be slower than 10 ms.

Residual dipolar couplings (RDCs) depend on the orientation of individual bond vectors with respect to each other and hence are very well suited to provide insight into the domain orientation of proteins in solution. For the major conformer of calexcitin, the NH RDCs were measured and used to determine the alignment tensors of the N-terminal and C-terminal domains individually using the X-ray structure as a reference for both domains, where α, β and γ represent the

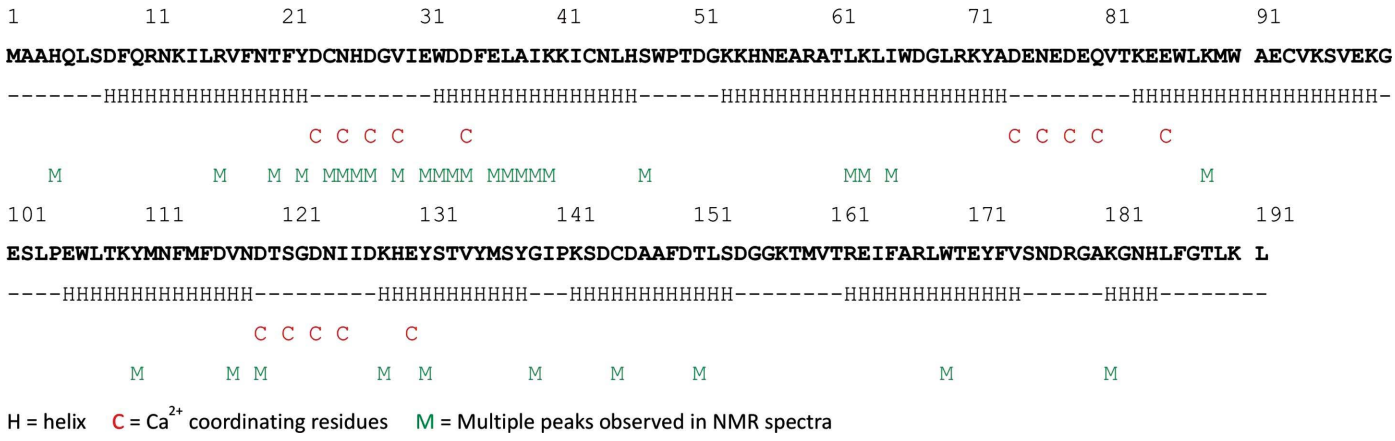

Figure 6
Assigned backbone amide NH NMR signals observed to exist in two states plotted against the calexcitin sequence. Not all signals from the minor conformation are necessarily detected owing to peak overlap or intermediate exchange effects. Helical structure and calcium-coordinating residues are highlighted.

Table 2
Results of the alignment-tensor determination for calexcitin in solution.

Calexcitin domain	α (°)	β (°)	γ (°)	A_a ($\times10^{-4}$)	A_r ($\times10^{-4}$)	χ^2 per residue	Q-factor
N-terminal domain	115.5 ± 3.0	149.3 ± 0.6	155.3 ± 1 0	−5.0 ± 0.1	−0.8 ± 0.1	15.0 ± 0.2	0.32
C-terminal domain	75.0 ± 1.9	147.9 ± 0.6	157.8 ± 0.7	−5.8 ± 0.1	−1.6 ± 0.1	24.7 ± 0.2	0.33

Euler angles of the three-dimensional coordinate axis of the domain with respect to the frame of the X-ray coordinates (PDB entry 2ccm; Erskine *et al.*, 2006) and A_a and A_r represent the axial and rhombic components of the molecular alignment tensor (Table 2). If the solution structure agrees with the crystal structure, the orientations of the alignment tensors of both domains would be expected to be the same. While the angles β and γ of both domains agree quite well, the α angles differ by about 40°. Accordingly, a model of the solution structure was created in which the two domains of calexcitin (N-domain, residues 2–101; C-domain, residues 102–191) were rotated by 40° in order to satisfy the domain alignment calculated from the RDC data. This creates a more open structure as illustrated by the superposition of the N-terminal domains of the model and the calexcitin crystal structure shown in Figs. 7(*a*) and 7(*b*).

The dynamics of calexcitin were investigated using NMR by measuring the longitudinal (T_1) and transverse (T_2) relaxation times of the backbone amide N atoms. A plot of T_1 *versus* T_2 (Fig. 8*a*) reveals that most residues have similar relaxation times and hence report similar rotational correlation times. This is indicative of a well structured protein without significant local mobility on the subnanosecond timescale. Only residues at the termini show additional fast internal motion as indicated by a longer T_2 (Fig. 8*b*). The N-terminal and C-terminal domains tumble in solution with correlation times of 10.6 and 10.0 ns, respectively, which are smaller than the 12.3 ns correlation time predicted using *HYDRONMR* for calexcitin (PDB entry 2ccm) and the 14.3 ns correlation time predicted for the more open RDC-derived model of the solution structure. Since the experimental data yield a smaller correlation time than the predictions from a rigid structure, we conclude that this is a result of interdomain motion on a nanosecond timescale (Rooney *et al.*, 2004). Such motion reduces the T_1 values and consequently a number of residues show T_1/T_2 values outside the theory-derived $S^2 = 1$ curve. In addition, smaller than calculated T_2 values may reflect contributions to the line width from aggregation effects. However, two residues, Trp169 and Lys190, show clear signs of line broadening, *i.e.* small T_2 values that are indicative of motion on the microsecond–millisecond time scale. Residues in calexcitin exhibiting two conformational states, weak peak intensity and/or short T_2 have been mapped to the structure in Fig. 9 and are coloured blue, orange and green, respectively. Interestingly, the Trp169 side chain was observed to adopt very different conformations in

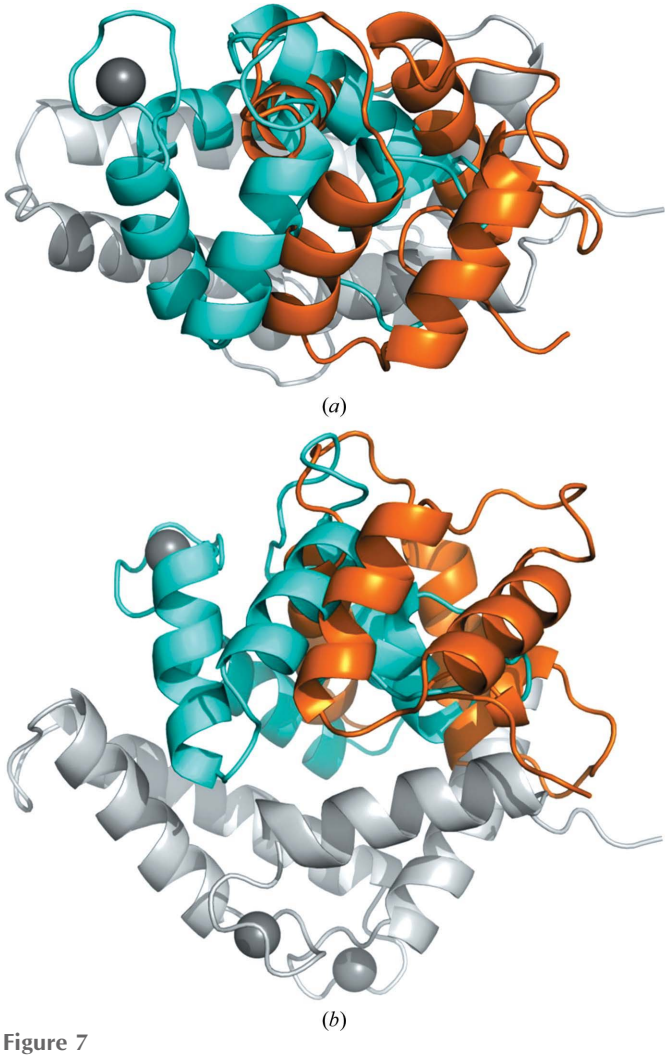

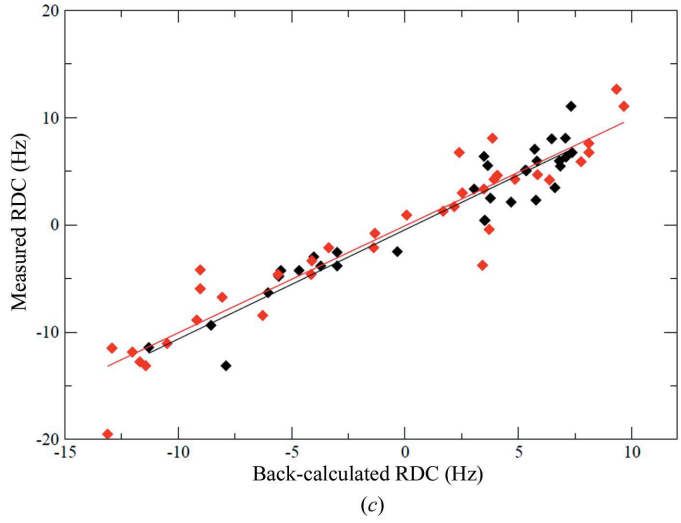

Figure 7
Domain orientation of calexcitin in solution. (*a*) Superimposition of the N-terminal domain of the major conformer (orange) on the calexcitin crystal structure (white, N-terminal domain; cyan, C-terminal domain) illustrating the rigid-body rotation that must be applied to the C-terminal domain in order to satisfy the RDC data acquired for calexcitin in the solution state. (*b*) The same as in (*a*) but rotated through 90°. (*c*) Plot of measured RDC values *versus* those back-calculated from the solution-state model.

the two molecules within the crystallographic asymmetric unit in the original structural analysis of calexcitin (Erskine *et al.*, 2006).

Interactions of calexcitin with the peptide mimicking the putative recognition site in the ryanodine receptor as well as with GTP and the nonhydrolyzable analogue GDPNP were investigated by titration up to a 20:1 maximum ratio of ligand to protein. In both cases no significant chemical shift changes were observed in the ^{15}N HSQC NMR spectra whether in the presence or absence of exogenous calcium.

3.5. Rigidity in calexcitin: wild-type and T188D mutant structures

We have examined the rigidity of the calexcitin structure using pebble-game rigidity analysis (Jacobs *et al.*, 2001), a rapid integer algorithm for matching degrees of freedom against constraints, using the freely available *FIRST* software package. In this approach the constraint network includes covalent and hydrophobic tether interactions, as well as a user-controlled set of polar interactions. Potential hydrogen-bond and salt-bridge interactions are assigned a bond energy based on the donor–hydrogen–acceptor geometry; an energy cutoff parameter $E_{\rm cut}$ then selects the interactions to include in the constraint network. Comparison of the rigidity at different values of $E_{\rm cut}$ provides information on the relative rigidity (and hence, the potential flexibility) of different regions of the protein.

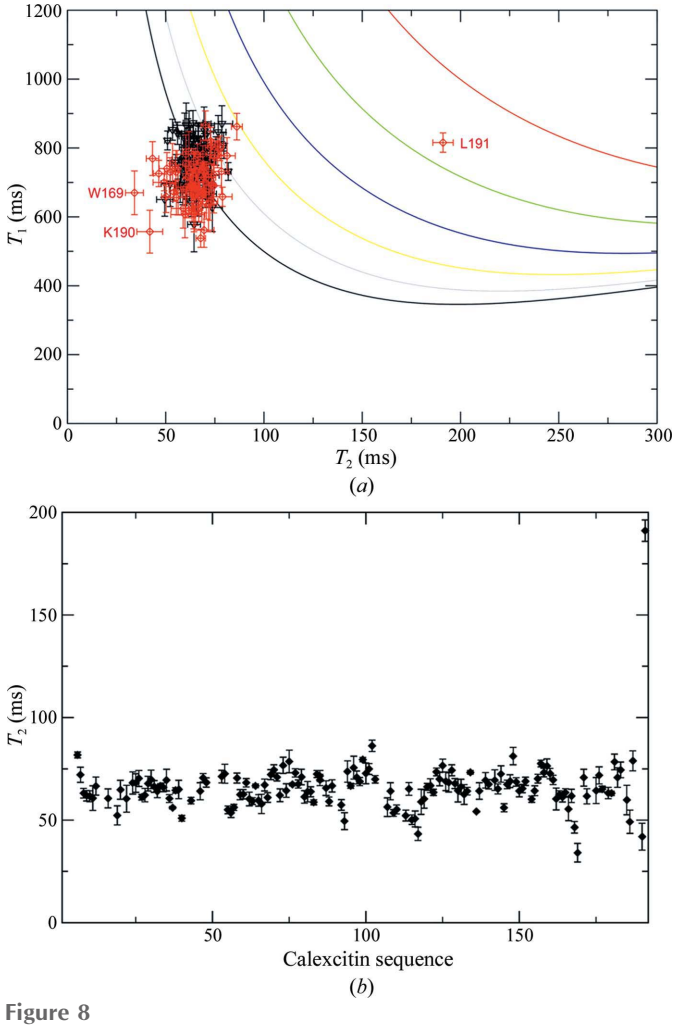

Figure 8
Backbone dynamics of calexcitin. (*a*) Parameterized plot of T_1 *versus* T_2 relaxation times with different order parameters S^2 (green, $S^2 = 1$; purple, $S^2 = 0.9$; grey, $S^2 = 0.8$; brown, $S^2 = 0.7$; yellow, $S^2 = 0.6$; blue, $S^2 = 0.5$) using the Lipari–Szabo model-free approach. Measured T_1 and T_2 relaxation times for each backbone N atom in calexcitin are shown as open rectangles. Residues in the N-terminal domain are in black and those in the C-terminal domain are in red. (*b*) A plot of T_2 relaxation times *versus* calexcitin sequence. Calexcitin appears to be relatively rigid with little fast internal motion. The dynamics are dominated by a slow conformational exchange between two unequally populated states.

Figs. 10(*a*), 10(*b*), 10(*c*) and 10(*d*) shows the rigid cluster decomposition of wild-type calexcitin at $E_{\rm cut}$ values of −1, −2, −3 and −4 kcal mol^{-1}, respectively. The overall behaviour of the protein is typical for a largely α-helical structure (Wells *et al.*, 2009). At small cutoff values the protein forms a single large rigid cluster, while as the cutoff is lowered flexibility develops and rigidity is lost, first from loop regions and then from α-helical regions. At large cutoff values the structure is largely flexible and only a few helices remain as separate rigid clusters. It is notable that the C-terminal region, near the phosphorylation site around residue 188 and the 3_{10}-helix, is one of the first portions of the structure to become flexible, consistent with the suggestion that rearrangements in this area may occur and be significant for function. The nearby first N-terminal helix, by contrast, is one of the most rigid regions in the protein.

The T188D phosphorylation-mimic mutant structure has comparable resolution to the wild-type structure and displays some side-chain rearrangements in the area around the mutation site, although the protein backbone geometry is very similar to the wild-type structure. Figs. 10(*e*), 10(*f*), 10(*g*) and 10(*h*) show the rigid cluster decomposition of T188D calexcitin at $E_{\rm cut}$ values of −1, −2, −3 and −4 kcal mol^{-1}, respectively, for comparison with the wild type. The mutant

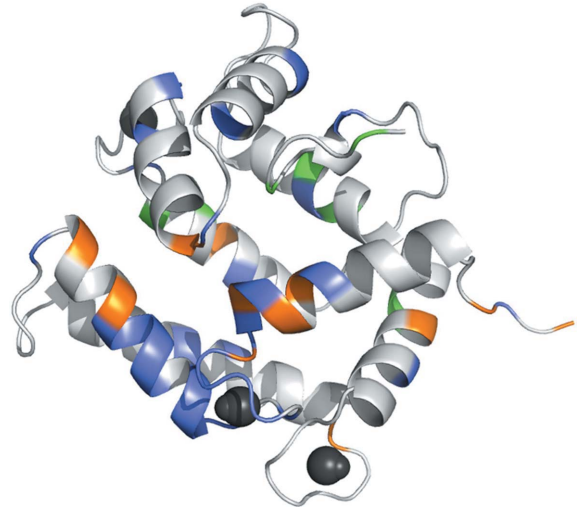

Figure 9
Overview of residues in calexcitin exhibiting two conformational states (blue), weak peak intensity (orange) and short T_2 (green). Each calcium ion and the associated water molecule is shown as a dark-grey sphere.

structure displays a decrease in rigidity compared with the wild-type case, in the sense that groups of α-helices forming a single rigid cluster in the wild-type protein are separate rigid clusters in the mutant structure; compare Figs. 10(*b*) and 10(*c*) with Figs. 10(*f*) and 10(*g*) to observe this effect at $E_{\rm cut}$ values of -2 and -3 kcal mol^{-1}. The increased flexibility is not localized to the mutation site but is observed across the structure, as rigidity is not a purely local phenomenon.

3.6. Noncovalent interactions linking the N-terminal and C-terminal domains

The NMR data indicate that in solution calexcitin exists not only in the compact conformation observed in the crystal structure but also in a more open state with the opening of a large cleft separating the N-terminal and C-terminal domains. It is therefore of interest to examine the set of noncovalent constraints linking the two domains in the wild-type structure, as it is this set which must be disrupted in the formation of the more open structure.

Examination of the constraint network identified by *FIRST* shows a relative paucity of noncovalent interactions linking the two domains. The central part of the cleft between the domains does not contain hydrophobic or strong polar interactions. The interdomain interactions are instead found on either side of the central cleft, particularly between the helices closest to the linking region around residue 102. The noncovalent interdomain contacts are mostly hydrophobic, with only a few strong polar interactions. The noncovalent inter-

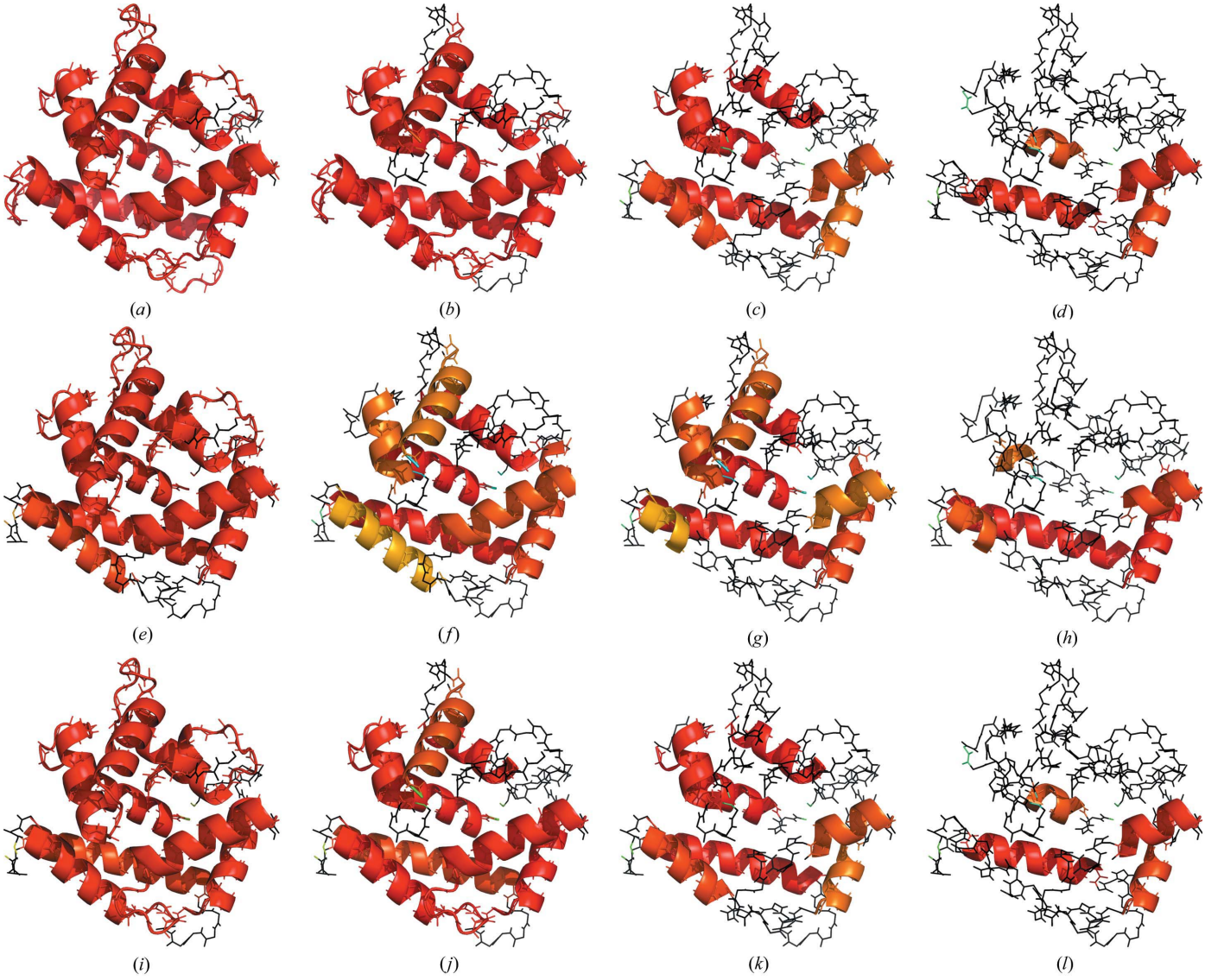

Figure 10
Rigid clusters identified in calexcitin crystal structures by pebble-game rigidity analysis. The protein main chain is shown in stick representation with large rigid clusters shown in cartoon form. Rigid clusters 1–20 are coloured in a spectrum from red to blue. (*a*), (*b*), (*c*) and (*d*): rigid clusters in wild-type calexcitin, with constraint networks including polar interactions stronger than -1, -2, -3 and -4 kcal mol^{-1}, respectively. (*e*), (*f*), (*g*) and (*h*): rigid clusters in T188D mutant calexcitin, with constraint networks including polar interactions stronger than -1, -2, -3 and -4 kcal mol^{-1}, respectively. (*i*), (*j*), (*k*) and (*l*): rigid clusters in wild-type calexcitin, excluding all interactions between N-terminal residues (up to residue 102) and C-terminal residues (residues 103 onwards).

Table 3
Noncovalent interactions identified by *FIRST* between the N-terminal and C-terminal domains in the wild-type calexcitin crystal structure.

Residues in bold are involved in noncovalent interactions with three or more other residues. Multipliers (×*N*) signify multiple interactions between the given pair of residues.

Hydrophobic interactions		Polar (hydrogen-bond) interactions		
C-terminal residue	N-terminal residue	C-terminal residue	N-terminal residue	Energy (kcal mol^{-1})
Phe9	Leu191	Ser7	Asn176	−0.780
Phe9	Arg178	Gln10	Val174	−1.912
Lys13	Leu189	**Lys13**	Ser175	−4.662
Lys13	**Tyr172**	**Lys13**	Glu171	−0.229
Val17	Phe173	**Lys13**	**Tyr172** (×2)	−2.285, −1.171
Val17	**Tyr172**	**Lys13**	Asn183	−3.231
Val17	Phe186	Arg16	Tyr172	−3.232
Phe21	Tyr138 (×2)	Arg16	Phe186	−0.957
Phe21	Tyr135 (×2)	His46	Val117	−4.277
Phe21	Phe186			
Ile42	Phe113			
Ala58	Phe113			
Ile65	Lys109			
Ile65	Tyr110 (×2)			
Leu69	Trp106			
Tyr72	Pro104 (×2)			
Met89	Trp106			
Trp90	Leu107 (×2)			
Trp90	Phe173 (×3)			
Cys93	Pro104			
Val97	Val174			
Val97	Leu103			

actions are shown in Table 3 and Fig. 11. A small number of residues, particularly Lys13, Val17, Phe21, Tyr172 and Trp90, have a 'keystone' role in the constraint network, forming interactions with multiple other residues, and these residues are emphasized in Fig. 11. This brings out in particular the strong, multiple hydrophobic tether links between the first N-terminal helix and the last C-terminal helices.

All of these interdomain interactions must be disrupted in the formation of the more open structure. It is interesting to note that the phosphorylation site at residue 61, which is not itself directly involved in the interdomain constraint network, lies close to a cluster of hydrophobic interactions linking the domains. This suggests that an increase in the hydrophilicity at this site, owing to the addition of the highly soluble charged phosphate group, would favour the entry of solvent water molecules into the interdomain cleft and the disruption of the nearby hydrophobic tether network.

We examined the effect of disruption of the interdomain noncovalent constraints by calculating the rigid cluster decomposition of the wild-type calexcitin structure with the interdomain constraints manually removed from the constraint network. The results are shown in Figs. 10(*i*), 10(*j*), 10(*k*) and 10(*l*). The rigid clusters formed in this case are almost identical to those formed in the wild-type structure (compare Figs. 10*a*–10*d*). It thus appears that the interdomain noncovalent constraints do not make a substantial contribution to the structural rigidity of the N-terminal and C-terminal domains. This provides further justification for the treatment of calexcitin as a two-domain protein and is consistent with the NMR data indicating that the N-terminal and C-terminal domains remain individually well constrained but can separate from each other by a cleft-opening motion in solution.

3.7. Normal-mode biased geometric simulations of flexible motion in calexcitin

We have explored the capacity for flexible motion of the calexcitin structure using template-based geometric simulations as implemented in the *FRODA* module (Wells *et al.*, 2005) of the *FIRST* software. This approach implements motion in a fully detailed (all-atom) protein structure with a simplified, localized physical model including the covalent bonding geometry, steric exclusion and the noncovalent interaction network identified by *FIRST*. Recent work in methods development (Ahmed *et al.*, 2011; Jimenez-Roldan *et al.*, 2012) has shown that it is particularly effective to explore motion biased along low-frequency normal-mode eigenvectors. The combined use of *FIRST*/*FRODA* with the *ElNémo* elastic network modelling software (Suhre & Sanejouand, 2004) has proved to be very successful as a generator of structure-based hypotheses for data interpretation in applications as diverse as protein–drug (calmodulin–cisplatin) interactions (Li *et al.*, 2012), large-scale domain reorientation (Amin *et al.*, 2013) and functional motion in citrate synthase (Wells *et al.*, 2014).

We have applied the *FIRST*/*FRODA* + *ElNémo* approach (Jimenez-Roldan *et al.*, 2012) to explore flexible motion in both the wild-type and T188D mutant calexcitin structures. In each case eigenvectors were calculated for the ten lowest frequency nontrivial normal modes. The eigenvectors thus generated were very similar for the wild-type and mutant

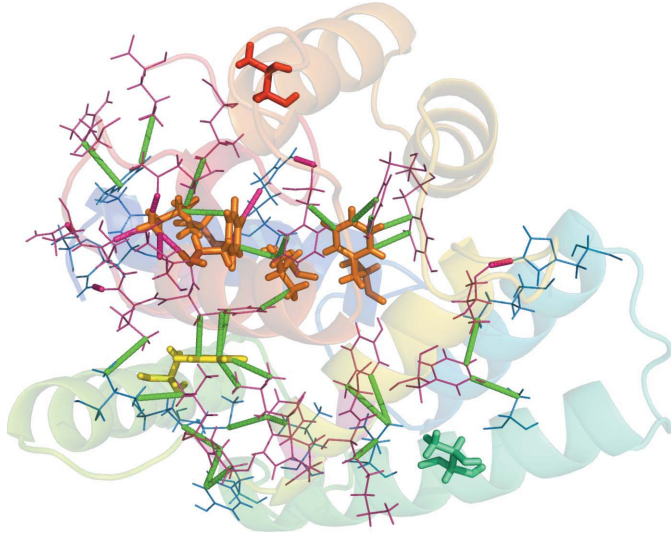

Figure 11
Polar (purple) and hydrophobic (green) interactions between residues in the N-terminal and C-terminal domains of wild-type calexcitin, as listed in Table 3. The main chain is shown in transparent cartoon representation; interacting residues are shown as thin sticks coloured light blue (N-terminal residues) or light pink (C-terminal residues). Thicker stick representation highlights residues involved in interdomain interactions with three or more other residues (orange), residue Trp90 (yellow), which makes multiple interactions with two C-terminal domain residues, and the phosphorylation sites at residues 61 (blue, bottom of image) and 188 (red, top of image).

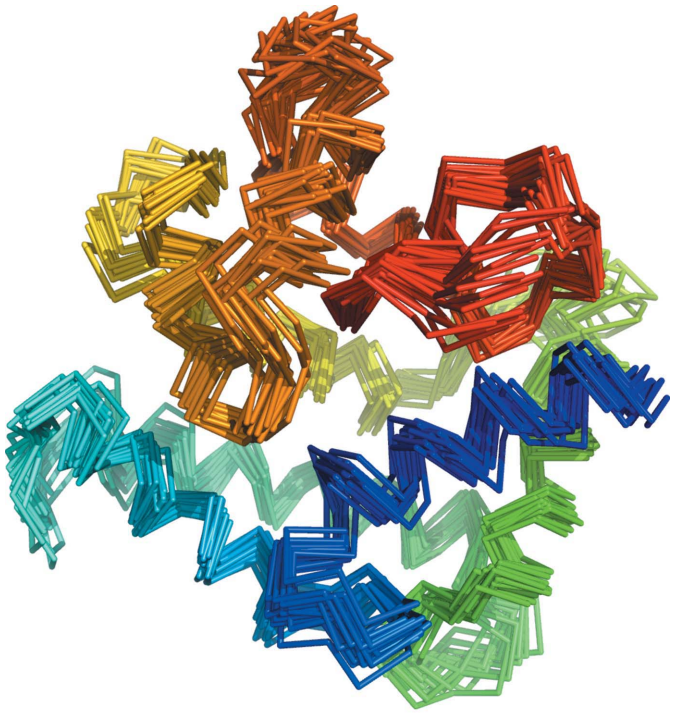

(*a*)

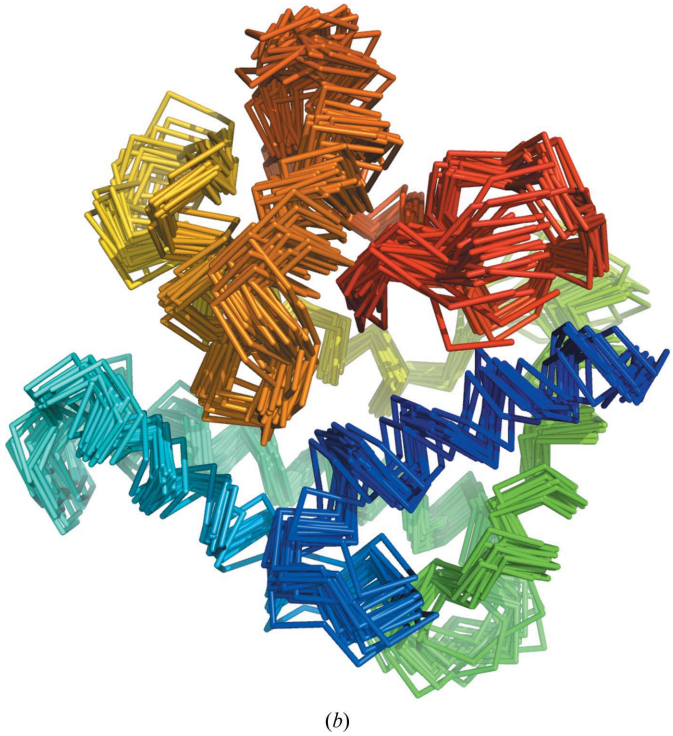

(*b*)

Figure 12
Normal-mode dynamics in wild-type (*a*) and T188D mutant (*b*) calexcitin structures. In each case the ribbon bundle shows the main-chain geometry of conformers generated by geometric simulations which are biased parallel and antiparallel to the ten lowest frequency nontrivial normal modes (7–16) until the amplitude is limited by steric or noncovalent interaction constraints. The chain is 'rainbowed' from blue (N-terminus) to red (C-terminus). Simulations include residues 6–191; *i.e.* residues 1–5 were omitted as otherwise multiple modes localize on the N-terminal tail. The T188D structure displays a slightly greater range of flexible motion, particularly around the C-terminal region (orange and red) and the nearby N-terminal helix (dark blue).

structures owing to the similarity of the backbone geometry. Motion was explored with biases parallel and antiparallel to each mode eigenvector, making a total of 20 trajectories for each structure. All modes were explored to the limits of 'easy motion' (Jimenez-Roldan *et al.*, 2012), thus finding the amplitudes at which flexible motion becomes limited by the steric and noncovalent constraints in the structure. Fig. 12 shows an overlay of 20 structures representing this envelope of flexible motion for the wild-type structure (Fig. 12*a*) and the T188D phosphorylation mimic mutant (Fig. 12*b*). The mutant structure was found to have a greater range of motion in the C-terminal region around the mutation site. Interestingly, this greater conformational freedom is transmitted to other parts of the structure, including the first N-terminal helix. These results are consistent with the suggestion that phosphorylation of residue 188 favours greater conformational freedom in the region of the protein associated with putative GTPase activity.

On closer examination of the character of the lowest frequency nontrivial normal-mode eigenvector (mode 7), it appears that the mode includes some cleft-opening character; that is, residues in the N-terminal domain on one side of the interdomain cleft have components of motion oppositely directed to those in the C-terminal domain on the other side of the interdomain cleft. We have carried out simulations of motion biased along this mode eigenvector with the interdomain noncovalent constraints eliminated. Fig. 13 shows an overlay of a structure from the resulting trajectory with the

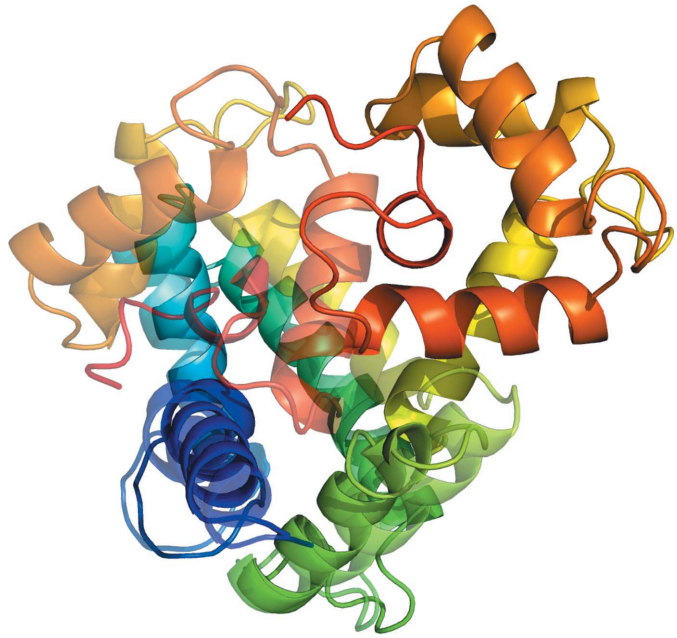

Figure 13
Wild-type calexcitin structure projected by geometric simulation biased along the lowest frequency nontrivial mode (mode 7) in the absence of noncovalent constraints linking residues in the N-terminal and C-terminal domains. The structure is projected from the starting state (semi-transparent cartoon) to a much more open state comparable to that identified by solution NMR (solid cartoon) by pivoting about the linker region around residue 102. Structures are aligned on the N-terminal domain to highlight the relative motion of the C-terminal domain as the cleft opens.

input wild-type structure. Motion along this mode in the absence of interdomain constraints leads to substantial opening of the cleft and a relative motion of the C-terminal and N-terminal domains comparable in scale to that observed in the NMR results.

4. Discussion

There are several reports that calexcitin is a calcium-activated GTPase, although efforts to co-crystallize the protein with GTP and nonhydrolyzable analogues have been unsuccessful, as have extensive NMR studies of GTP binding. However, mutagenesis studies have identified a number of residues that appear to be important for the reported GTPase activity (Nelson *et al.*, 2003). These include Gly182, Phe186 and Gly187 and a number of neighbouring amino acids that occur in or are immediately adjacent to a region of 3_{10}-helix (helix 9) at the C-terminus. This short helix is packed between helices 7 and 8 in the C-terminal domain and helix 1 in the N-terminal domain (Fig. 1). The fact that helices 7 and 8 form the nonfunctional EF-hand of the protein suggests that during evolution the calcium-binding properties of this helix–loop–helix motif may have been sacrificed to provide a GTP-binding subdomain. The 3_{10}-helix occurs at the extremely hydrophobic interface between the two domains of the protein which are likely to separate upon binding of target molecules. Thus, it is likely that calexcitin would also have to undergo a conformational change in order to bind GTP. Interestingly, there is clear evidence that this part of the buried interdomain core has marked fluidity, which is reflected in our observations of the conformational disorder of certain side chains. The proximity of site 3 to the putative GTP-binding region of the protein, which includes the C-terminal 3_{10}-helix (residues 181–185), might therefore allow the GTPase activity of calexcitin to be regulated by calcium binding to the low-affinity sensory site of the protein. Interestingly, the homologous protein juvenile hormone diol kinase, which uses GTP or ATP to phosphorylate insect juvenile hormone, is inhibited by low concentrations of calcium ions (Li *et al.*, 2005).

Phosphorylation of calexcitin by PKC is reported to cause its translocation to the cell membrane, where its effects on potassium channels are exerted (Nelson *et al.*, 1996). Calexcitin has two PKC phosphorylation sites at positions Thr61 and Thr188. The first of these, Thr61, is approximately in the centre of helix 3 and is roughly equidistant from the second and third calcium-binding sites (approximately 20 Å). There are no conserved basic residues in the vicinity of Thr61 that might interact with a phosphate group, and the distance of this residue from the calcium-binding sites suggests that phosphorylation may not affect their affinity very much. However, assuming that calexcitin interacts with target proteins in a similar manner to calmodulin, the proximity of Thr61 to the hydrophobic interface between the N-terminal and C-terminal domains suggests that phosphorylation may alter both the equilibrium between its open and closed forms and its affinity for target proteins. The proximity of the other phosphorylated residue, Thr188, to the C-terminal end of the protein means that it is also close to the interface between the N-terminal and C-terminal domains, and thus phosphorylation of this residue may also have an effect on domain opening. This residue is close to a salt bridge formed between Asp144 and Lys190 and is also close to His184 in the C-terminal 3_{10}-helix (helix 9) and a number of other basic residues. Thus, phosphorylation of Thr188 could have a significant effect on the local conformation of the protein in a region that has been implicated in its putative GTPase activity. This has indeed been conformed by our structural studies, which showed marked local rearrangements of protein side chains in the vicinity of this phosphorylation-mimic mutation.

In the simulation studies, the presence of a cleft-opening component in the lowest frequency nontrivial mode of motion may be a reflection in the elastic network model of the protein of the same phenomenon as observed in the constraint network: a relative absence of interactions between the N-terminal and C-terminal domains in the interior of the interdomain cleft. Thus, our various computational investigations concur with the NMR results on this point that the calexcitin structure, even though it seems to form a single compact unit in the crystal structure, is in fact two separately well constrained domains with a substantial capacity for relative flexible motion and the opening of an interdomain cleft. The exposure of hydrophobic surfaces during cleft opening would offer a route for calexcitin to interact with and regulate other proteins in a manner similar to that observed for calmodulin, which binds to other proteins through the opening of methionine-rich hydrophobic clefts.

Acknowledgements

We thank the BBSRC for a studentship to AB and a project grant to BAW. We are indebted to the ESRF, Grenoble, France and Diamond Light Source, Didcot, England for beam time and travel support. We would also like to thank the Wellcome Trust (grant 090658/Z/09/Z) for support of the Southampton NMR centre and the MRC for support of the Biomedical NMR Centre at Mill Hill (grant No. U117533887). SAW acknowledges support from EPSRC project grant EP/K004956/1. SAW and JBC acknowledge CCP5 for travel support.

References

Ahmed, A., Rippmann, F., Barnickel, G. & Gohlke, H. (2011). *J. Chem. Inf. Model.* **51**, 1604–1622.
Alkon, D. L. & Nelson, T. J. (1990). *FASEB J.* **4**, 1567–1576.
Amin, N. T., Wallis, A. K., Wells, S. A., Rowe, M. L., Williamson, R. A., Howard, M. J. & Freedman, R. B. (2013). *Biochem. J.* **450**, 321–332.
Ascoli, G. A., Luu, K. X., Olds, J. L., Nelson, T. J., Gusev, P. A., Bertucci, C., Bramanti, E., Raffaelli, A., Salvadori, P. & Alkon, D. L. (1997). *J. Biol. Chem.* **272**, 24771–24779.
Beaven, G. D. E., Erskine, P. T., Wright, J. N., Mohammed, F., Gill, R., Wood, S. P., Vernon, J., Giese, K. P. & Cooper, J. B. (2005). *Acta Cryst.* F**61**, 879–881.
Bers, D. M., Patton, C. W. & Nuccitelli, R. (1994). *Methods Cell Biol.* **40**, 3–29.
Cavallaro, S., Meiri, N., Yi, C.-L., Musco, S., Ma, W., Goldberg, J. & Alkon, D. L. (1997). *Proc. Natl Acad. Sci. USA*, **94**, 9669–9673.

Chen, V. B., Arendall, W. B., Headd, J. J., Keedy, D. A., Immormino, R. M., Kapral, G. J., Murray, L. W., Richardson, J. S. & Richardson, D. C. (2010). *Acta Cryst.* D**66**, 12–21.
Cook, W. J., Jeffrey, L. C., Cox, J. A. & Vijay-Kumar, S. (1993). *J. Mol. Biol.* **229**, 461–471.
Delaglio, F., Grzesiek, S., Vuister, G. W., Zhu, G., Pfeifer, J. & Bax, A. (1995). *J. Biomol. NMR*, **6**, 277–293.
Emsley, P. & Cowtan, K. (2004). *Acta Cryst.* D**60**, 2126–2132.
Erskine, P. T., Beaven, G. D. E., Hagan, R., Findlow, I. S., Werner, J. M., Wood, S. P., Vernon, J., Giese, K. P., Fox, G. & Cooper, J. B. (2006). *J. Mol. Biol.* **357**, 1536–1547.
Evans, P. (2006). *Acta Cryst.* D**62**, 72–82.
Farrow, N. A., Muhandiram, R., Singer, A. U., Pascal, S. M., Kay, C. M., Gish, G., Shoelson, S. E., Pawson, T., Forman-Kay, J. D. & Kay, L. E. (1994). *Biochemistry*, **33**, 5984–6003.
García de la Torre, J., Huertas, M. L. & Carrasco, B. (2000). *J. Magn. Reson.* **147**, 138–146.
Gombos, Z., Jeromin, A., Mal, T. K., Chakrabartty, A. & Ikura, M. (2001). *J. Biol. Chem.* **276**, 22529–22536.
Grzesiek, S. & Bax, A. (1992). *J. Am. Chem. Soc.* **114**, 6291–6293.
Hashimoto, Y., Kohri, K., Kaneko, Y., Morisaki, H., Kato, T., Ikeda, K. & Nakanishi, M. (1998). *J. Biol. Chem.* **273**, 16544–16550.
Jacobs, D. J., Rader, A. J., Kuhn, L. A. & Thorpe, M. F. (2001). *Proteins*, **44**, 150–165.
Jimenez-Roldan, J. E., Freedman, R. B., Römer, R. A. & Wells, S. A. (2012). *Phys. Biol.* **9**, 016008.
Johnson, B. A. & Blevins, R. A. (1994). *J. Biomol. NMR*, **4**, 603–614.
Karplus, P. A. & Diederichs, K. (2012). *Science*, **336**, 1030–1033.
Kay, L. E., Nicholson, L. K., Delaglio, F., Bax, A. & Torchia, D. A. (1992). *J. Magn. Reson.* **97**, 359–375.
Kay, L. E., Xu, G. Y. & Yamazaki, T. (1994). *J. Magn. Reson. A*, **109**, 129–133.
Laskowski, R. A., MacArthur, M. W., Moss, D. S. & Thornton, J. M. (1993). *J. Appl. Cryst.* **26**, 283–291.
Lees, J. G., Miles, A. J., Wien, F. & Wallace, B. A. (2006). *Bioinformatics*, **22**, 1955–1962.
Lees, J. G., Smith, B. R., Wien, F., Miles, A. J. & Wallace, B. A. (2004). *Anal. Biochem.* **332**, 285–289.
Leslie, A. G. W. (2006). *Acta Cryst.* D**62**, 48–57.
Li, H., Wells, S. A., Jimenez-Roldan, J. E., Römer, R. A., Zhao, Y., Sadler, P. J. & O'Connor, P. B. (2012). *Protein Sci.* **21**, 1269–1279.
Li, S., Zhang, Q.-R., Xu, W.-H. & Schooley, D. A. (2005). *Insect Biochem. Mol. Biol.* **35**, 1235–1248.
Lovell, S. C., Davis, I. W., Arendall, B., de Bakker, P. I. W., Word, J. M., Prisant, M. G., Richardson, J. S. & Richardson, D. C. (2003). *Proteins*, **50**, 437–450.
Martin, S. R., Maune, J. F., Beckingham, K. & Bayley, P. M. (1992). *Eur. J. Biochem.* **205**, 1107–1117.
Maune, J. F., Beckingham, K., Martin, S. R. & Bayley, P. M. (1992). *Biochemistry*, **31**, 7779–7786.
Maune, J. F., Klee, C. B. & Beckingham, K. (1992). *J. Biol. Chem.* **267**, 5286–5295.
Maxwell, R. A., Welch, W. H., Horodyski, F. M., Schegg, K. M. & Schooley, D. A. (2002). *J. Biol. Chem.* **277**, 21882–21890.
Maxwell, R. A., Welch, W. H. & Schooley, D. A. (2002). *J. Biol. Chem.* **277**, 21874–21881.
Miles, A. J., Wien, F., Lees, J. G., Rodger, A., Janes, R. W. & Wallace, B. A. (2003). *Spectroscopy*, **17**, 653–661.
Minakami, R., Jinnai, N. & Sugiyama, H. (1997). *J. Biol. Chem.* **272**, 20291–20298.
Murshudov, G. N., Skubák, P., Lebedev, A. A., Pannu, N. S., Steiner, R. A., Nicholls, R. A., Winn, M. D., Long, F. & Vagin, A. A. (2011). *Acta Cryst.* D**67**, 355–367.
Nakajima, Y., Yamamoto, T., Nakayama, T. & Nakanishi, S. (1999). *J. Biol. Chem.* **274**, 27573–27577.
Nelson, T. J. & Alkon, D. (1995). *J. Neurochem.* **65**, 2350–2357.
Nelson, T. J., Cavallaro, S., Yi, C.-L., McPhie, D., Schreurs, B. G., Gusev, P. A., Favit, A., Zohar, O., Kim, J., Beushausen, S., Ascoli, G., Olds, J., Neve, R. & Alkon, D. L. (1996). *Proc. Natl Acad. Sci. USA*, **93**, 13808–13813.
Nelson, T. J., Collin, C. & Alkon, D. L. (1990). *Science*, **247**, 1479–1483.
Nelson, T. J., Quattrone, A., Kim, J., Pacini, A., Cesati, V. & Alkon, D. L. (2003). *Comp. Biochem. Physiol. B*, **135**, 627–638.
Nelson, T. J., Yoshioka, T., Toyoshima, S., Fan, Y.-F. & Alkon, D. L. (1994). *Proc. Natl Acad. Sci. USA*, **91**, 9287–9291.
Nelson, T. J., Zhao, W.-Q., Yuan, S., Favit, A., Pozzo-Miller, L. & Alkon, D. H. (1999). *Biochem. J.* **341**, 423–433.
Ottiger, M., Delaglio, F. & Bax, A. (1998). *J. Magn. Reson.* **131**, 373–378.
Rhoads, A. R. & Friedberg, F. (1997). *FASEB J.* **11**, 331–340.
Rooney, L. M., Sachchidanand & Werner, J. M. (2004). *Methods Mol. Biol.* **278**, 123–138.
Sheldrick, G. M. & Schneider, T. R. (1997). *Methods Enzymol.* **277**, 319–343.
Sreerama, N., Venyaminov, S. Y. & Woody, R. W. (1999). *Protein Sci.* **8**, 370–380.
Sreerama, N. & Woody, R. W. (2000). *Anal. Biochem.* **287**, 252–260.
Starovasnik, M. A., Klevit, R. E., Su, D.-R. & Beckingham, K. (1991). *Protein Sci.* **1**, 245–253.
Stokkum, I. H. M. van, Spoelder, H. J. W., Bloemendal, M., van Grondelle, R. & Groen, F. C. A. (1990). *Anal. Biochem.* **191**, 110–118.
Suhre, K. & Sanejouand, Y.-H. (2004). *Nucleic Acids Res.*, **32**, W610–W614.
Vagin, A. & Teplyakov, A. (2010). *Acta Cryst.* D**66**, 22–25.
Vaguine, A. A., Richelle, J. & Wodak, S. J. (1999). *Acta Cryst.* D**55**, 191–205.
Vijay-Kumar, S. & Cook, W. J. (1992). *J. Mol. Biol.* **224**, 413–426.
Wells, S. A., Crennell, S. J. & Danson, M. J. (2014). *Proteins*, **82**, 2657–2670.
Wells, S. A., Jimenez-Roldan, J. E. & Römer, R. A. (2009). *Phys. Biol.* **6**, 046005.
Wells, S. A., Menor, S., Hespenheide, B. & Thorpe, M. F. (2005). *Phys. Biol.* **2**, S127–S136.
Whitmore, L. & Wallace, B. A. (2008). *Biopolymers*, **89**, 392–400.
Winn, M. D. *et al.* (2011). *Acta Cryst.* D**67**, 235–242.
Wittekind, M. & Mueller, L. (1993). *J. Magn. Reson. B*, **101**, 201–205.